White Rose Research Online

eprints@whiterose.ac.uk
https://eprints.whiterose.ac.uk
Universities of Leeds, Sheffield and York

Deposited via The University of Leeds.

White Rose Research Online URL for this paper:
https://eprints.whiterose.ac.uk/id/eprint/80332/

Version: Submitted Version

Article:
Geboy, NJ, Kaufman, AJ, Walker, RJ et al. (2013) Re-Os age constraints and new observations of Proterozoic glacial deposits in the Vazante Group, Brazil. Precambrian Research, 238. 199 - 213. ISSN: 0301-9268

https://doi.org/10.1016/j.precamres.2013.10.010

Reuse
Items deposited in White Rose Research Online are protected by copyright, with all rights reserved unless indicated otherwise. They may be downloaded and/or printed for private study, or other acts as permitted by national copyright laws. The publisher or other rights holders may allow further reproduction and re-use of the full text version. This is indicated by the licence information on the White Rose Research Online record for the item.

Takedown
If you consider content in White Rose Research Online to be in breach of UK law, please notify us by emailing eprints@whiterose.ac.uk including the URL of the record and the reason for the withdrawal request.

UNIVERSITY OF LEEDS
University of Sheffield
UNIVERSITY of York

Re-Os age constraints and new observations of Proterozoic glacial deposits in the Vazante Group, Brazil

Nicholas J. Geboy[1], Alan J. Kaufman[2,3], Richard J. Walker[2], Aroldo Misi[4], Tolentino Flavio de Oliviera[5], Kristen E. Miller[6], Karem Azmy[7], Brian Kendall[8], and Simon W. Poulton[9]

1. United States Geological Survey, Reston, VA 20192, USA
2. University of Maryland, Department of Geology, College Park, MD 20742, USA
3. University of Maryland, Earth System Science Interdisciplinary Center, College Park, MD 20742, USA
4. Centro de Pesquisa em Geofísica e Geologia, Universidade Federal da Bahia (CPGG/UFBA), CEP 40170-290 Salvador-Bahia, Brazil
5. Independent consultant, Rio de Janeiro RJ, Brazil
6. Massachusetts Institute of Technology, Department of Earth, Atmospheric and Planetary Sciences, Cambridge, MA 02139, USA
7. Department of Earth Sciences, Memorial University of Newfoundland, St. John's, Newfoundland A1B 3X5, Canada
8. University of Waterloo, Department of Earth and Environmental Sciences, Waterloo, Ontario N2L 3G1, CANADA
9. University of Leeds, School of Earth and Environment, Leeds LS2 9JT, United Kingdom

ABSTRACT

A new Re-Os radiometric age date for an organic-rich shale horizon from the Vazante Group in Brazil, coupled with geological observations, provide evidence for late Mesoproterozoic glacial episodes, conflicting with the general view of greenhouse conditions marked by a eustatic high stand at this time. Field observations of a reverse fault juxtaposing older Mesoproterozoic sedimentary rocks above younger Neoproterozoic strata provide a new stratigraphic framework and reconcile the apparent inversion of U-Pb detrital zircon ages through the succession. Combined, the geochronological, geochemical and

stratigraphic evidence suggest that the Vazante Group sediments accumulated along a passive margin of the São Francisco craton and are correlative with the neighboring Paranoá Group. Biomarker, sulfur isotope and iron speciation analyses support the interpretation of a strongly stratified water column during post-glacial transgression and deposition of one of the bituminous shale horizons. The relationship of the glaciogenic Vazante Group to other late Mesoproterozoic successions, such as the non-glacial Atar Group in West Africa and Bylot Supergroup in arctic Canada, however, remains enigmatic.

Key words: Vazante Group; Mesoproterozoic glaciation; Re-Os geochronology; Fe-speciation

1. Introduction

The Precambrian geologic record contains evidence of widespread ice ages, including diamictite left behind by melting glaciers, capped by texturally and isotopically anomalous carbonate and organic-rich shale that accumulated in the wake of rising sea levels (Harland and Bidgood, 1959; Kaufman et al., 1991; Kirschvink, 1992; Kennedy 1996; Hoffman et al., 1998; Schrag et al., 2002; Bekker et al., 2005). Existing age constraints suggest that these Precambrian ice ages were episodic rather than continuous, with a series of temporally discrete glaciation events occurring at the beginning and end of the Proterozoic Eon (*cf.* Kaufman et al., 1997; Kennedy et al., 1998; Walter et al., 2000; Kendall et al., 2004; 2006) but with little evidence of glaciation in the intervening billion years.

Due to the general lack of radiometric determinations on sedimentary successions, however, the absolute ages of many of the Proterozoic diamictites are poorly known. To advance understanding of the tempo and mode of these ancient ice ages, researchers have applied a geochronometer based on the radioactive decay of ^{187}Re to ^{187}Os, most commonly on samples of organic-rich shale preserved in drill cores (Kendall et al., 2004; 2006; Azmy et al., 2008; Rooney et al., 2010) or syn-depositional sulfide grains (Hannah et al., 2004). Published results for Neoproterozoic (1.0-0.542 Ga) successions support the view that the Sturtian and Marinoan glacial epochs represented multiple discrete ice ages over a protracted time frame (*cf.* Kaufman et al., 1997). Contrary to expectations, a Re-Os study of a dropstone-

54 laden shale horizon from the Vazante Group in south-central Brazil (Azmy et al., 2008) indicated a late
55 Mesoproterozoic age – a time previously believed to have been ice free.
56 In this paper, we re-evaluate the stratigraphic position of this shale, which was previously
57 interpreted to be syn-glacial in origin (Olcott et al., 2005) and support the Mesoproterozoic age with new
58 Re-Os work from a second shale horizon unrelated to glacial deposits, as well as identify a thrust fault
59 lower in the Vazante Group that juxtaposes older Mesoproterozoic strata above younger glaciogenic
60 sedimentary rocks of Neoproterozoic age. Detrital zircon U-Pb constraints for the Vazante Group
61 (Rodrigues et al., 2012), coupled with carbon and strontium isotope data and paleontological evidence,
62 are consistent with the stratigraphic inversion and our Re-Os age determinations.
63
64 **2. Geologic and Geochronologic Background**
65 The Vazante Group is a sedimentary succession that occurs in wide swaths atop the eastern part
66 of the Brasília Fold Belt (BFB) on the western margin of the São Francisco craton throughout Minas
67 Gerais, Brazil (Fig. 1). Surface outcrops are strongly weathered and the succession has been exposed to
68 sub-greenschist facies metamorphism (Babinski et al., 2005; Azmy et al., 2008), but well preserved
69 carbonate and organic-rich shale are available in drill core. Figure 2 shows a generalized stratigraphy of
70 the Vazante Group, including three potential glacial horizons, as well as the reverse fault located near the
71 town of Lagamar (Pinho and Dardenne, 1994), which resulted in older strata of the Vazante Group –
72 including the shale horizons studied here – to overly younger sedimentary rocks (see Section 5.1 for
73 further details and implications). The basal Vazante diamictite (St. Antônio do Bonito Formation) has
74 long been interpreted as glacial in origin based on the presence of faceted and striated cobbles of mixed
75 lithology, including basement clasts, floating in a mudstone matrix (Dardenne, 2000). The two upper
76 Vazante Group diamictites at the base of the Morro do Calcário and Lapa formations are characterized by
77 carbonate breccia or laminated shale disrupted by carbonate dropstones. Further evidence for a glacial
78 origin for the two upper Vazante diamictites includes: 1) their widespread distribution across the basin; 2)
79 the observation that cobbles and boulders in the Morro do Calcário (previously attributed to the Serra do

Poço Verde Formation) are both rounded and angular, with the rounded stones often faceted (Fig. 3A, B); 3) the thick black Morro do Calcário shale contains glendonite, a pseudomorph of ikaite, a carbonate mineral that forms in organic-rich sediment at temperatures between -1.9 to 7°C (*cf.* Olcott et al., 2005); 4) the uppermost strata of the Lapa diamictite are Fe-oxide cemented with local accumulations of iron-formation (*cf.* Derry et al., 1992; Kaufman et al., 1997; Hoffman et al., 1998); and 5) the carbonates and marl overlying both diamictites preserve negative $\delta^{13}C$ excursions typical of post-glacial cap carbonates (Azmy et al., 2001; 2006; Brody et al., 2004).

The three shale horizons sampled for Re-Os analysis in this study were from, in ascending order, the pre-glacial Serra do Garrote Formation and the post-glacial Morro do Calcário and Lapa formations. The Serra do Garrote Formation consists of dark grey shale hundreds of meters thick that has been metamorphosed to a greenish slate in some areas; the shale can be carbonaceous and/or pyrite bearing (Dardenne, 2000). The Morro do Calcário and Lapa formations are both composed of laminated shale and dolostone, which contain intermittent ice-rafted debris and based on core observations are each several hundred meters thick (Dardenne, 2000). The true thickness of these units, however, is difficult to ascertain insofar as outcrops are discontinuous and coupled with the likelihood of tectonic repetition of strata due to thrust faulting. The Morro do Calcário and Lapa formations accumulated during post-glacial transgression over sub-glacial valleys largely filled with carbonate breccia. Sub-glacial unconformities cut through underlying carbonate platform deposits of the Serra do Poço Verde and Morro do Calcário formations (indicated by the heavier formation-boundary lines in Fig. 2); in some cores it appears that the two upper Vazante Group diamictites are in direct contact while in others they are separated by a variety of bedded lithologies.

The age of the Vazante Group is controversial. Cloud and Dardenne (1973) argued that the presence of the stromatolite *Conophyton metula Kirichenko* (Fig. 3C) near the base of the Lagamar Formation suggests an age ranging between 1350 and 950 Ma. Stromatolite biostratigraphy, however, is poorly constrained and competing tectonic models suggest a Neoproterozoic initiation of Vazante Group sedimentation either in a rapidly subsiding foreland basin associated with the Brasíliano collision (*ca*. 790

106 Ma; Dardenne, 2000) or along a passive continental margin during supercontinent breakup (*ca*. 900 Ma;
107 Pimentel et al., 2001). Whole rock Rb-Sr data for a Vazante Group shale yielded an isochron age of ~600
108 Ma, but this age likely represents a date related to Brasíliano metamorphism (Amaral and Kawashita,
109 1967). A Neoproterozoic age for the upper Vazante Group was suggested based on a comparison of time-
110 series isotope trends (Azmy et al., 2001), although an alternative interpretation of these variations
111 suggested an older potential age for the succession (Misi et al., 2007). Most recently, Re-Os dates of 993
112 ± 46 and 1100 ± 77 Ma (excluding Re- and Os-poor samples) were determined from a dropstone-laden
113 shale in the Vazante Group previously believed to be part of the Lapa Formation (Azmy et al., 2008) but
114 here is assigned to the Morro do Calcário Formation (see below).
115
116 **3. Methods**
117 All samples were taken from two pristine drill cores provided by Votorantim Metais. For Re-Os
118 analysis, samples were selected from the Serra do Garrote Formation in drill hole 134-86, from roughly
119 coeval horizons of the Morro do Calcário Formation in drill holes 42-88 and 134-86 and from the Lapa
120 Formation in drill hole 134-86. The upper two shale horizons in core 134-86 are separated by a thick
121 interval of carbonate breccia, quartzite and iron-cemented diamictite (Brody et al., 2004). In 2009, we re-
122 examined this core and concluded that the shale horizon Azmy et al. (2008) studied from drill hole
123 MASW-01 belonged to the Morro do Calcário Formation, rather than the Lapa Formation as previously
124 discussed.
125
126 *3.1 Re/Os*
127 The Re-Os system can provide precise depositional ages for organic-rich shale because these
128 facies are often deposited in anoxic environments where Re and, to a lesser extent, Os may be sequestered
129 from seawater in their reduced states and incorporated into organic matter (Ravizza and Turekian, 1989;
130 Cohen et al., 1999; Selby and Creaser, 2003; Kendall et al., 2004). Once incorporated in the sediment,
131 ^{187}Re undergoes beta decay to ^{187}Os with a half-life of approximately ~42 Ga. With the assumption that

all of the shale samples in a suite have the same initial osmium isotopic composition (from coeval seawater) and a wide range in parent:daughter ratios, it is possible to generate an isochron, which yields the age of incorporation of Re and Os into the system and, hence, of deposition. Since shale facies contain both hydrogenous and terrigenous components, it is necessary to digest the samples with a less-aggressive medium, such as Cr^{VI}-H_2SO_4, which preferentially attacks the organic component while leaving the detrital quartz and feldspar largely intact (Selby and Creaser, 2003).

Approximately 50 mg of powdered whole rock was accurately weighed along with a known quantity of a ^{190}Os-^{185}Re spike and Cr^{VI}-H_2SO_4 digestion solution (Selby and Creaser, 2003) and transferred to frozen Carius tubes that were chilled using a mixture of dry ice and ethanol before being sealed with an oxy-propane torch (Shirey and Walker, 1995). Once thawed, the Carius tubes were placed in an oven heated to 240°C for 48 hours to fully oxidize the Re and Os to their highest valence states. Following digestion, the tubes were frozen in liquid nitrogen and opened. The Os was separated from the mixture via solvent extraction using carbon tetrachloride, back extracted into HBr and purified by micro-distillation prior to being loaded onto a Pt filament and analyzed using negative thermal ionization mass spectrometry (N-TIMS; Birck et al., 1997; Cohen and Waters, 1996). Following Os separation, the remaining solution was treated with sulfurous acid to reduce the Cr^{6+} to Cr^{3+}, and Re was separated using anion exchange chromatography before being taken up in 2% nitric acid and analyzed using inductively coupled plasma mass spectrometry (ICP-MS). All of the preparation chemistry and spectrometry were conducted at the University of Maryland's Geochemical Laboratories. Samples were blank corrected, with total analytical blanks averaging 19 pg and < 1 pg for Re and Os, respectively. These blanks were sufficiently low as to have no effect on analytical uncertainties. Reproducibility was determined using a ^{185}Re spiked in-house standard of the Agpalilik iron meteorite, where $^{185}Re/^{187}Re = 1.331 \pm 0.002$ (n = 10; 2SDM) over a two-month measuring period and a UMD Os standard where $^{187}Os/^{188}Os = 0.1140 \pm 0.0003$ (n = 9; 2SDM) and $^{190}Os/^{192}Os = 1.981 \pm 0.002$ (n = 9; 2SDM) over a nine-month measuring period. Regressions were performed with *Isoplot V.4.15* (Ludwig, 2011) using a value of 1.666×10^{-11} yr^{-1} for the

157 ^{187}Re decay constant and 2σ uncertainties for $^{187}Re/^{188}Os$ and $^{187}Os/^{188}Os$ as determined by numerical
158 error propagation.
159
160 *3.2 Total Organic Carbon and Stable Isotopes*
161 Shale horizons were sampled from drill cores 134-86 and 42-88 for time-series analyses.
162 Samples were ground with a ceramic mortar and pestle and aliquots were used for measuring total organic
163 carbon (TOC) abundance, stable S and C isotope analyses, as well as Fe-speciation. TOC was determined
164 using Dumas combustion techniques on pre-acidified powders and quantified on a vacuum distillation
165 line. The $\delta^{13}C$ of the TOC was determined by combustion in a Eurovector elemental analyzer in-line with
166 an Isoprime gas source isotope ratio mass spectrometer (EA-IRMS). Sulfide sulfur in the shales was
167 isolated using a chrome-reduction solution (*cf*. Canfield et al., 1986) to release H_2S, which was carried in
168 a stream of nitrogen gas through a Milli-Q ultrapure water trap to remove chloride. Sulfur was then
169 trapped as Ag_2S with a 0.02 M solution of $AgNO_3$ and 1.55 M HNO_3. Silver sulfide solutions were set in
170 the dark for approximately seven days, then filtered and rinsed with ~250 ml Milli-Q water and ~5 ml 1N
171 ammonia solution (NH_4OH). Samples were aged to allow for the dissolution of oxygen-bearing
172 contaminants that precipitate with the silver sulfide. The black Ag_2S precipitate was then filtered and
173 dried for ~48 hours and combined with excess V_2O_5 in tin cups for EA-IRMS measurement of sulfur
174 isotope compositions. Uncertainties of carbon and sulfur isotope analyses based on multiple analyses of
175 urea and NBS-127 standards were better than 0.1 and 0.3‰, respectively.
176
177 *3.3 Fe-Speciation*
178 Iron-speciation analyses, based on measured abundances of Fe in carbonate, oxide and sulfide
179 mineral phases, as well as total Fe in samples, were conducted following procedures outlined by Poulton
180 and Canfield (2005). Sulfide iron abundance (Fe-S) is calculated from Ag_2S yields in CRS extractions
181 (see Section 3.2), performed sequentially after checking for Fe present as acid volatile sulfides. For the
182 carbonate and oxide fractions, fresh bulk powders are sequentially leached with: 1) 1 M sodium acetate

183 ($C_2H_3NaO_2$) adjusted to pH 4.5 with acetic acid (CH_3COOH) for 48 hours at 50°C to release carbonate
184 iron (Fecarb); 2) dithionite solution (mixture of 50 g L^{-1} sodium dithionite ($Na_2S_2O_4$), 0.2 M sodium
185 citrate ($Na_3C_6H_5O_7 \cdot H_2O$) and 0.35 M acetic acid) for two hours to release iron from ferric oxides such as
186 hematite and goethite (Feox); and 3) ammonium oxalate solution (mixture of 0.2 M ammonium oxalate
187 ($C_2H_8N_2O_4$) and 0.17 M oxalic acid ($H_2C_2O_4 \cdot H_2O$) for six hours to extract iron from magnetite (Fe_{mag}).
188 The iron extracted from carbonates, oxides and sulfides are combined to yield the highly reactive pool
189 (Fe_{HR}). This Fe_{HR} pool represents Fe minerals that are reactive towards dissolved sulfide on diagenetic
190 timescales (Canfield et al., 1992; Poulton et al., 2004a). Total iron concentrations (Fe_T) were determined
191 by total digestion with concentrated HF, HNO_3 and $HClO_4$. All Fe extracts were analysed by Flame
192 Atomic Adsorption Spectroscopy, with repeat analyses yielding RSD's of <5% for all stages.
193
194 **4. Results**
195
196 *4.1 Re-Os*
197 Results of Re and Os analyses for the Serra do Garrote, Morro do Calcário and Lapa formation
198 shales are reported in Table 1. In the Serra do Garrote samples, Re and Os concentrations ranged from ~1
199 to 16 ppb, and ~60 to 600 ppt, respectively. The isotopic data show a generally isochronous relationship
200 (Fig. 4A) indicating an age of 1354 ± 88 Ma (n = 8, MSWD = 49). Presuming the isochron age to be
201 accurate, the initial $^{187}Os/^{188}Os$ value (Os_i) of each sample is back-calculated. The reproducibility of Os_i
202 of individual samples in the Serra do Garrote shale (Table 1) suggests minimal post-depositional mobility
203 (Kendall et al., 2009). The Serra do Garrote date presented here is, admittedly, imprecise with a relatively
204 high MSWD value. However, the Os_i from the isochron regression falls between values of ~0.12
205 (chondritic/mantle compositions in the late Mesoproterozoic; Walker et al., 2002a, b) and 1.5 (riverine
206 inputs; Levasseur et al., 1999) that would reasonably be expected for seawater $^{187}Os/^{188}Os$. Such an
207 observation suggests that any post-depositional disturbance is relatively minor. The large uncertainty
208 (~5%) on the age may arise from changes in the initial Os isotopic composition of seawater during

deposition (data used to generate Fig. 4A come from samples spreading approximately 1.5 m of section). The changing Os isotopic composition of the source water and minor open-system behavior may also explain the relatively high MSWD value.

Rhenium and Os concentrations in the thick, organic-rich Morro do Calcário shale vary substantially between the two sampled cores, which were drilled ~2.3 km apart. Samples from drill core 42-88 contain between ~0.30 and 0.85 ppb Re and between ~27 and 55 ppt Os, while those from drill core 134-86 are characterized by higher concentrations with ~1 to 23 ppb Re and ~40 to 700 ppt Os. The differences are most likely related to environmental and facies variations, as metal abundances in the two cores are broadly correlated with that of total organic carbon, suggesting sedimentary controls on their distribution (Anbar et al., 2007). Sample sets from these two cores can be combined to yield a composite isochron with an age of 1112 ± 50 Ma (n = 16, MSWD = 91; Fig. 4B). Although care was taken to sample the two drill cores from roughly equivalent horizons, we cannot *a priori* assume that these horizons are directly contemporaneous, particularly as the data plot in two distinct positions along the isochron. Furthermore, the samples from drill core 42-88 have very low Re and Os abundances, and therefore may be more readily contaminated by detrital components of the shale (Azmy et al., 2008). Taking only the more metal enriched Morro do Calcário samples from drill core 134-86 results in an imprecise isochron age of 1035 ± 200 Ma (n = 8, MSWD = 150; Fig. 4C) with scatter that is greater than analytical uncertainties. Duplicate analyses of some samples gave minor to moderate differences in $^{187}Re/^{188}Os$ and $^{187}Os/^{188}Os$ and likely reflect variable extents of powder heterogeneity. While neither the composite isochron nor the drill core 134-86 isochron are strong enough to warrant a direct depositional age assignment, it is worth noting that both are statistically identical to the Morro do Calcário Formation's previously assigned Re-Os age (1100 ± 77 Ma; Azmy et al., 2008).

Samples from the thin Lapa Formation shale in core 134-86 have the lowest concentrations of both Re and Os in this study (Table 1), and exhibit a very limited range in $^{187}Re/^{188}Os$ and $^{187}Os/^{188}Os$. Hence, these samples do not define an isochron, and we do not consider the Lapa Formation measurements further.

235

236 *4.2 C-S*

237 Results for time-series C and S analyses from the Serra do Garrotte, Morro do Calcário and Lapa
238 formations sampled from drill core 134-86 and 42-88 are reported in Table 2 and illustrated in Figures 5
239 and 6. In core 134-86 (Fig. 5), where all three shale horizons were collected and analyzed, TOC
240 abundances range widely between 0 and 4 wt.% with highest overall (but variable) abundances in the
241 Morro do Calcário shale and in a singular peak within the Lapa shale. Carbon isotope compositions of
242 Serra do Garrotte samples range between -28 and -31‰, values similar to samples from the base of the
243 Morro do Calcário Formation. Stratigraphically higher in the Morro do Calcário, samples define a trend
244 of ^{13}C enrichment with $\delta^{13}C$ values reaching as high as -22‰. In contrast, organic matter in Lapa
245 Formation samples have relatively constant $\delta^{13}C$ values around -25‰. Sulfur isotope compositions in this
246 core were not measured for the Serra do Garrotte Formation. In the Morro do Calcário, sample $\delta^{34}S$
247 values range from +10 to -15‰, becoming more depleted in ^{34}S up-section. In contrast, Lapa Formation
248 samples are notably enriched in ^{34}S, ranging from +10 to +35‰, defining a positive excursion that peaks
249 in the most organic-rich horizons.

250 Morro do Calcário samples from core 42-88 (Fig. 6) were previously studied for biomarker
251 distributions and organic carbon contents (Olcott et al., 2005). TOC abundances in these samples range
252 up to 3.5 wt.%, with most samples having $\delta^{13}C$ values near to -25‰, regardless of organic carbon content.
253 Sulfur contents are similar to those of organic matter, ranging up to 3 wt.%, but $\delta^{34}S$ values define a
254 significant positive excursion with a progressive 20‰ rise in the lower half of the section to values as
255 high as approximately +30‰, which fall back to around +10‰ in the upper half of the section.

256

257 *4.3 Fe-speciation*

258 Iron-speciation analyses were conducted on the Morro do Calcário samples from core 42-88 (Fig.
259 6; Table 3) in order to better understand the redox architecture of the depositional basin and for

comparison with environmental interpretations from the previously published biomarker results. Fe_{HR}/Fe_T ratios can be used to distinguish oxic from anoxic water column depositional conditions, whereby values >0.38 provide strong support for anoxic deposition, while values <0.22 suggest oxic depositional water column conditions (Raiswell and Canfield, 1998; Poulton and Raiswell, 2002; Poulton and Canfield, 2011). For samples that show clear evidence for anoxic deposition, Fe-S/Fe_{HR} values >0.7-0.8 suggest euxinic deposition, while values below this threshold suggest anoxic non-sulfidic depositional conditions (Poulton et al., 2004b; Poulton and Canfield, 2011). Fe_{HR}/Fe_T ratios range widely through the formation (Fig. 6). Notably high values for samples at depths <759 m, between 785 and 812 m, and >825 m provide strong evidence for dominantly anoxic deposition across these intervals, perhaps with occasional transitions to oxic deposition from 800-812 m (potentially a consequence of fluctuations in the depth of the chemocline). In contrast, low Fe_{HR}/Fe_T from 759-785 m and 812-825 m depths suggests dominantly oxic water column conditions for these samples, although periodically higher Fe_{HR}/Fe_T ratios suggest the possibility of cycling between oxic and anoxic conditions. To distinguish anoxic non-sulfidic and euxinic deposition, Fe-S/Fe_{HR} ratios are plotted on Fig. 6 for samples which show evidence of anoxic deposition (i.e., Fe_{HR}/Fe_T >~0.38). In general, lower Fe-S/Fe_{HR} towards the top and bottom of the section implies anoxic non-sulfidic depositional conditions, while higher values in the middle portion of the section suggests dominantly euxinic conditions.

5. Discussion

Although the Re-Os isochron ages for upper Vazante shales determined previously (Azmy et al., 2008) and in this study are imprecise, they are consistent with a late Mesoproterozoic to earliest Neoproterozoic age assignment. This age for the Vazante Group contrasts with an earlier chemostratigraphic age estimate (Azmy et al., 2001; 2006), which was in part based on the assumption that all the glacial deposits must be from the Neoproterozoic Era.

5.1 Stratigraphic context for a Mesoproterozoic age of the upper Vazante Group

286 Detrital zircons from the middle of the Serra do Garrote and the top of the Morro do Calcário
287 formations yield U-Pb ages varying from 1505 to 2521 Ma and 1109 to 2466 Ma, respectively; lower in
288 the Serra do Garrote detrital zircon ages vary from 1242 to 3409 Ma (Rodrigues et al., 2012). Taken as
289 maximum depositional ages, these former dates do not contradict the Re-Os ages but do require relatively
290 rapid unroofing and transportation of the zircons. In contrast, younger detrital zircon U-Pb ages from
291 formations of the Vazante Group below the shale horizons (Azmy et al., 2008; Rodriguez et al., 2012) do
292 appear to contradict our Re-Os age estimates. For example, the Rocinha Formation contains zircons as
293 young as 930 Ma and the St. Antônio do Bonito Formation contains zircons with ages as young as ~1000
294 Ma (Azmy et al., 2008; Rodrigues et al., 2012), suggesting a likely Neoproterozoic age for this part of the
295 succession. In support of this view, Sr isotope compositions of phosphorite samples from the Rocinha
296 Formation (Fig. 3D), with $^{87}Sr/^{86}Sr$ values of 0.70766 (Misi et al., 2007), match those of the
297 Neoproterozoic Bambuí Group to the east on the São Francisco craton. The cap carbonate at the base of
298 that succession is constrained by a Pb-Pb carbonate age of 740 ± 22 Ma (n = 11; MSWD = 0.66; Babinski
299 et al., 2007).
300 These paradoxical observations are resolved by the presence of a 40-45° oblique-slip reverse fault
301 beneath outcrops of *Conophyton metula Kirichenko* stromatolite in the Lagamar Formation (Fig. 3E).
302 The fault is identified in aerial photographs and in the field by the presence of brown to yellow clay-rich
303 and sandy mylonite overlying thickly bedded purple shale (Fig. 3F). This reverse fault appears to
304 subdivide the Vazante Group into two parts; older sediments assigned to the Vazante Group are thrust
305 above younger carbonates and phosphates in the Rocinha Formation and the St. Antônio do Bonito
306 Formation glacial diamictite (Misi et al., 2010; 2011). Notably, the Vazante Formation (now Group)
307 originally defined by Dardenne (1978) did not include the basal Santo Antônio do Bonito and Rocinha
308 because these units were severely faulted relative to overlying strata. This tectonic transposition explains
309 many of the conflicting chronometric constraints on the Vazante Group and should be expected given the
310 imbrication of thrust nappes to the west and south in highly metamorphosed terrains (Dardenne, 2000).
311 Movement along this reverse fault – initiated by collision of continental blocks during the late-

312 Neoproterozoic (*ca*. 600 Ma) Brasíliano orogeny – places older strata above younger and separates the
313 Vazante Group into at least two distinct tectonic and sedimentary domains. If this interpretation is
314 correct, the basal Vazante Group diamictite would likely be equivalent to the glacial deposits at the base
315 of the Neoproterozoic Bambuí Group, leaving the two glacial deposits above the thrust fault to be the only
316 radiometrically constrained glaciogenic deposits of the Mesoproterozoic Era. The possibility of
317 additional, yet unrecognized, reverse faults in the Vazante Group cannot be discounted, which may
318 explain the slightly younger U-Pb ages observed in detrital zircons in the lower part of the Serra do
319 Garrote Formation (Rodrigues et al., 2012).
320
321 *5.2 Regional and depositional setting of the Vazante Group*
322 Two different tectonic models have been proposed to explain the accumulation of Vazante Group
323 strata. In one, Vazante sediments are suggested to have been deposited in a rapidly subsiding foreland
324 basin initiated during collision of the BFB with the flat-lying São Francisco craton at *ca.* 790 Ma
325 (Dardenne, 2000). This suggests a Neoproterozoic age for the succession. However, accepting the Re-Os
326 and U-Pb detrital zircon age constraints, as well as the presence of a major reverse fault within the
327 Vazante succession, it is most likely that only the Rocinha Formation and St. Antônio do Bonito
328 diamictite are correlative with Neoproterozoic deposits on the São Francisco craton (Misi et al., 2010;
329 2011).
330 In contrast, upper Vazante Group strata that accumulated on a passive margin carbonate platform
331 are of Mesoproterozoic age and likely correlative with the Paranoá Group (Fig 1) consistent with the
332 interpreted model based on Nd isotopic measurements of detrital grains from a variety of formations
333 across the BFB (Pimentel et al., 2001). The Nd-isotope measurements suggest a likely source of
334 sediments to the Vazante Group was from either the São Francisco craton to the east (T_{DM} ranging from
335 ~2.3 to 1.7 Ga) or the off-shore Goiás Magmatic Arc to the west (T_{DM} ranging from ~1.0 to 1.3 Ga). The
336 initial Nd isotopic compositions of detrital grains from the Serra do Garrote and Serra do Poço Verde
337 formations are identical to those from the nearby Paranoá Group, supporting their direct equivalence

(Pimentel et al., 2001). The Paranoá Group lacks direct radiometric constraints but is broadly constrained to between 1200 and 900 Ma (albeit based on stromatolite biostratigraphy; Dardenne et al., 1976). The Paranoá Group sits stratigraphically below the Bambuí Group, and glacial deposits have also been observed at its base (Dardenne, 2000). Carbonates in both the Vazante and Paranoá groups reveal relatively little $\delta^{13}C$ variation (Santos et al., 2000; Azmy et al., 2001). The pattern of relatively muted carbon isotope compositions through these successions stands in sharp contrast with Neoproterozoic carbonates of the Bambuí Group which exhibit a striking upsection trend in $\delta^{13}C$ values progressing from as low as -5‰ near its base in a cap carbonate lithofacies to near +15‰ at its top in bituminous limestones (Misi et al., 2007).

Previous biomarker studies of the Morro do Calcário shale (Olcott et al., 2005) interpreted this unit to be syn-glacial based on its appearance between thick carbonate diamictite and ample evidence of ice rafted debris. We currently recognize this organic-rich shale as related to post-glacial transgression with a stratigraphic placement between two carbonate diamictites of different age. Extractable biomarkers (including n-alkanes, isoprenoids, steranes and hopanes from shale, carbonate and diamictite) in the Morro do Calcário shale were interpreted to be indigenous to the sediments and reflect a complex microbial ecosystem, including both phototrophic bacteria and eukaryotes living in a stratified ocean with thin or absent sea ice, oxic surface waters and euxinic conditions within the photic zone (Olcott et al., 2005). Our Fe-speciation and S isotope results from the Morro do Calcário shale are consistent with these findings. The partitioning of Fe phases in these ancient sediments suggest that redox conditions in the depositional environment fluctuated on relatively short timescales between anoxic, euxinic and oxic water column conditions as the Morro do Calcário sediments accumulated, supporting the view of initial progressive stratification of the water column followed by generally more expansive ventilation. The dramatic enrichment in ^{34}S of pyrite in the lower part of the sampled interval may thus be interpreted in terms of progressive sulfate-limitation as the water column became increasingly euxinic. Our re-evaluation of this shale as a post-glacial (rather than syn-glacial) deposit, however, complicates our ability

363 to predict aspects of the ice age as they relate to biological productivity and diversity (*cf.* Olcott et al.,
364 2005; Corsetti et al., 2006).
365
366 *5.3 The Vazante Group in the context of a late Mesoproterozoic world*
367 The upper part of the Vazante Group (as originally described by Dardenne, 2000) is thus far the
368 only radiometrically constrained Mesoproterozoic succession preserving lithological and geochemical
369 evidence of glaciation, so caution about its global significance is warranted. Other studies of late
370 Mesoproterozoic strata indicate that this was a period of a global greenhouse conditions marked by
371 eustatic highstand (Kah et al., 1999; 2012; Gilleaudeau and Kah, 2013). This conundrum may be
372 explained by one of three scenarios: 1) the diamictites of the upper section of the Vazante Group have
373 been mis-identified as glaciogenic; 2) the Re-Os system has been perturbed or mis-interpreted, and the
374 apparent isochron ages do not reflect the timing of deposition; or 3) the Vazante Group accurately
375 captures a previously unobserved component of the late Mesoproterozoic Earth.
376 There is strong evidence that units within these strata are the result of multiple discrete glacial
377 events. Glaciation is the most likely mechanism that unites the geology (faceted and striated dropstones
378 along with iron-formation), mineralogy (glendonite) and geochemistry (negative $\delta^{13}C$ excursions) of the
379 upper Vazante Group diamictites. Citing these lines of evidence, this study is not the first to have
380 interpreted glacial strata within the Vazante Group (*cf*. Dardenne, 2001; Azmy et al., 2001; Brody et al.,
381 2004; Olcott et al., 2005; Azmy et al., 2006; Misi et al., 2007). However, the Vazante Group diamictites
382 have commonly been interpreted as correlative with Neoproterozic "snowball Earth" deposits found atop
383 the São Francisco craton (Misi et al., 2005) and the conjugate Congo craton (Azmy et al., 2001; 2006). If
384 the Re-Os ages are correct, these correlations will need to be revised. These new data do not warrant
385 altering the interpretation of glacial episodes within the Vazante Group, merely their timing.
386 The Re-Os system in organic-rich shale has been shown to be fairly robust. It appears
387 unperturbed by low-grade metamorphism (Kendall et al., 2004) and hydrocarbon maturation and
388 expulsion (Creaser et al., 2002) but can be disturbed by surface weathering (Jaffe et al., 2002). The

389 Vazante Group has been exposed to only sub-greenschist faces metamorphism (Babinksi et al., 2005;
390 Azmy et al., 2008) in the outcrop region. Furthermore, we sampled from unweathered and well-preserved
391 cores (Azmy et al., 2006). While it is possible for detrital components of the shale to contaminate the
392 hydrogenous Re-Os signatures and thereby influence the isochron ages, we used the Cr^{VI}-H_2SO_4 digestion
393 medium that preferentially attacks the hydrogenous component of the shale over detrital input (Selby and
394 Creaser, 2003; Kendall et al., 2004). Hydrothermal fluid flow can disturb Re-Os systematics but
395 documented cases of remobilization of Re and Os under such conditions have resulted in erroneously
396 *younger*, not older, ages (Kendall et al., 2009). Therefore, even with hydrothermal perturbation, the Serra
397 do Garrote and Morro do Calcário glaciations would not be correlative with the younger, globally
398 distributed Neoproterozoic events.
399 If the detrital input includes organic matter – as suggested for the post-glacial shale of the Morro
400 do Calcário Formation (Marshall et al., 2009) – then preferential digestion of hydrogenous components
401 may result in mixing of authigenic and detrital components and complicated Re-Os systematics. It seems
402 unlikely, however, that such a mixing process would have a consistently wide-spread impact (both
403 temporally and spatially) and result in isochronous relationships. Moreover, the Vazante stata Re-Os
404 dates presented here are in stratigraphic agreement with one another, over a time scale of hundreds of
405 millions of years, and derived from cores drilled approximately three kilometers apart. Furthermore,
406 while the Morro do Calcário shale is clearly related to glacial phenomenon, the Serra do Garrote shale is
407 not and thus detrital organic matter contamination through weathering inputs (*cf.* Johnston et al., 2012)
408 should be considerably less significant.
409 The abundance and wide geographic spread of open marine and epicratonic carbonate platform
410 deposits from the Mesoproterozoic, including the Bangemall Group (Buick et al., 1995), the Turukhansk
411 Group (Knoll et al., 1995; Bartley et al., 2001), the Society Cliffs Formation (Kah et al., 2001) and the
412 Atar Group (Kah et al., 2012) support the view of a world with globally high sea levels. Notably, the
413 carbon isotope records of these successions are characterized by relatively little variation, predominantly
414 ranging between -4‰ and +4‰, with shifts generally not exceeding 5‰ (Kah et al., 1999; Bartley et al.,

2001; Bartley et al., 2007; Kah et al., 2012; Gilleaudeau and Kah, 2013). This record stands in stark contrast to the succeeding Neoproterozoic when carbon isotope compositions of marine proxies reveal significant overall ^{13}C enrichments and high amplitude variations (Knoll et al., 1986; Kaufman and Knoll, 1995; Kaufman et al., 1997; Prave et al., 2009; Halverson et al., 2010).

As mentioned above, carbon isotope compositions of marine carbonates in the Vazante Group reveal a moderate spread in $\delta^{13}C$ values, largely falling within the range of -4‰ to +3‰ (Azmy et al., 2006). This range is consistent with other late Mesoproterozoic successions lacking evidence for glaciation (e.g. Kah et al., 1999). Stratigraphically coherent negative carbon isotope excursions in these successions have recently been explained as a result of relative sea level highstands, which promote anoxia and organic matter remineralization in epicratonic environment (Gilleaudeau and Kah, 2013). In contrast, the upper Vazante Group displays two consistent basin-wide negative shifts of up to 8‰ immediately above the interpreted glacial units (Azmy et al., 2006). Furthermore, the positive S isotope excursion captured in the lower Morro do Calcário shale, which occurs over just 20 meters of section (Fig. 6) is similar in magnitude to an event recorded from late Mesoproterozoic bedded sulfates on Baffin Island (Kah et al., 2004). This biogeochemical anomaly is best explained as the result of widespread removal of sulfate (via bacterial sulfate reduction) from an ocean that was relatively sulfate-poor (Canfield, 1998; Kah et al., 2004).

Given the uncertainties of the Re-Os ages presented here and previously (Azmy et al., 2008) and lack of geochronometric constraints in most other late Mesoproterozoic basins, it seems possible that the interval was environmentally variable or that there was a strong temperature gradient between the poles and equator. Paleomagnetic reconstructions place the São Francisco craton at high southern latitudes (45 to over 60° S) in the late Mesoproterozoic (Weil et al., 1998; Tohver et al., 2006), allowing the possibility that the glaciations of the Morro do Calcário and Serra do Garrote formations were local rather than global in extent.

Re-Os age estimates from the Touirist and En Nesoar formations of the Atar Group are statistically identical to the Morro do Calcário Formation (~1100 Ma; Rooney et al., 2010). The

similarity of these ages (and Os_i values) as well as their carbon isotopic records have led to the suggestion that these units were deposited coevally atop the West African and São Francisco cratons, respectively (Rooney et al., 2010). Although some aspects of the geochemistry and radiometric constraints are consistent with this hypothesis, the two successions were clearly deposited under conflicting climatic conditions causing other researchers (Kah et al., 2012) to question this correlation. Alternatively, the imprecise age for the Morro do Calcário (Azmy et al., 2008) allow the possibility that Vazante glaciogenic units are younger than the Touirist and En Nesoar formations of the Atar Group. Given the incision of the glacial units into the underlying carbonate platforms (Fig. 2), the Morro do Calcário and Lapa formations may document more substantial sea-level falls following Mesoproterozoic highstands captured elsewhere. Lacking a wider range of sedimentary units from this time period for comparison, it may not be possible to reconcile the Atar Group and other contemporary basins with the Vazante Group until more precise age constraints are available.

6. Conclusions

Based on our geological and radiometric study of Vazante Group strata in south-central Brazil, we conclude that the upper 2/3 of the succession was deposited on a passive margin of the São Francisco craton during the late Mesoproterozoic Era. The Re-Os radiometric ages for the Serra do Garrote (1345 ± 88 Ma; this study) and Morro do Calcário (1100 ± 77 Ma; Azmy et al., 2008) are consistent with previous estimates for upper Vazante strata based on the U-Pb age distributions of detrital zircons. Paleontological and carbon isotopic constraints also support a correlation of the upper section of the Vazante Group (above the Lagamar fault) with the Paranoá Group (also atop the São Francisco Craton), but not the Neoproterozoic Bambuí Group as suggested by earlier authors.

Evidence of two discrete glacial episodes in the upper part of the Vazante stratigraphy is preserved as 1) discrete diamictite horizons bearing both angular and rounded, faceted and striated clasts, sometimes preserved as dropstones in laminated shale; 2) the presence of the cold-water carbonate

466 mineral glendonite within one of the post-glacial shale horizons; 3) Fe-oxide cementation and local
467 accumulation of iron-formation; and 4) negative $\delta^{13}C$ excursion in carbonate overlying the diamictites.
468 Furthermore, we have identified map and field evidence for an oblique-slip reverse fault that
469 juxtaposes Neoproterozoic glaciogenic strata of the lower Vazante Group (Rocinha and St. Antônio do
470 Bonito) beneath late Mesoproterozoic formations of the upper Vazante Group, including the Serra do
471 Garrote, Morro do Calcário and Lapa units evaluated in this geochemical study. While the fault solves
472 the paradoxical U-Pb maximum depositional ages derived from detrital zircons and the stratigraphic
473 inversion, it also opens up the possibility of other, yet undiscovered, faults within the sequence which
474 may further complicate stratigraphic relationships.
475 The Vazante Group is unique in the late Mesoproterozoic in that it displays evidence of glaciation
476 in a period generally regarded as a time of greenhouse conditions and globally high sea levels. The
477 glaciations may be regional phenomena as paleo-reconstructions place the São Francisco craton at high
478 southern latitudes during the late Mesoproterozoic Era, but the general lack of open marine successions
479 from this time interval limits our current understanding of this ancient episode of Earth history.
480

481 **Acknowledgments**

482 The authors wish to thank Kristina Bartlett Brody and Natalie Sievers at the University of
483 Maryland for assistance with analyses and Julio Pinho for help in the field. We also thank Votorantim
484 Metais for access to the drill core samples. This work was partly funded by the National Science
485 Foundation and the Natural Research Council of Brazil. Comments from Ruth Schulte and Jim Coleman
486 of the USGS, Julie Bartley, Linda Kah and Geoff Gilleaudeau, as well as two anonymous reviewers
487 appointed by the journal greatly improved this paper. Any use of trade, firm, or product names is for
488 descriptive purposes only and does not imply endorsement by the U.S. Government.
489

490 **References Cited**

491 Amaral, G., Kawashita, K., 1967. Determinacao da idade do Grupo Bambui pelo metado Rb/Sr. Anais
492 21st Congresso Brasileiro Geologia Curitiba, Brasil, pp. 214-217.
493 Anbar, A.D., Duan, Y., Lyons, T.W., Arnold, G.L., Kendall, B., Creaser, R.A., Kaufman, A.J., Gordon,
494 G.W., Scott, C., Garvin, J., Buick, R., 2007. A whiff of oxygen before the Great Oxidation
495 Event? Science 317, 1903-1906.
496 Azmy, K., Kaufman, A.J., Misi, A., de Oliveira, T.F., 2006. Isotope stratigraphy of the Lapa Formation,
497 São Francisco Basin, Brazil: Implications for Late Neoproterozoic glacial events in South
498 America. Precambrian Res 149, 231-248.
499 Azmy, K., Kendall, B., Creaser, R.A., Heaman, L., de Oliveira, T.F., 2008. Global correlation of the
500 Vazante Group, São Francisco Basin, Brazil: Re-Os and U-Pb radiometric age constraints.
501 Precambrian Res 164, 160-172.
502 Azmy, K., Veizer, J., Misi, A., de Oliveira, T.F., Sanches, A.L., Dardenne, M.A., 2001. Dolomitization
503 and isotope stratigraphy of the Vazante Formation, Sao Francisco Basin, Brazil. Precambrian
504 Res 112, 303-329.
505 Babinski, M., Monteiro, L.S., Fetter, A.H., Bettencourt, J.S., Oliveira, T.F., 2005. Isotope geochemistry
506 of the mafic dikes from the Vazante nonsulfide zinc deposit, Brazil. J S Am Earth Sci 18, 293-
507 304.
508 Babinski, M., Vieira, L.C., Trinidade, R.I.F., 2007. Direct dating of the Sete Lagoas cap carbonate
509 (Bambuí Group, Brazil) and implications for the Neoproterozoic glacial events. Terra Nova 19,
510 401-406.
511 Bartley, J.K., Kah, L.C., McWilliams, J.L., Stagner, A.F., 2007. Carbon isotope chemostratigraphy of the
512 Middle Riphean type section (Avzyan Formation, Southern Urals, Russia): Signal recovery in a
513 fold-and-thrust belt. Chem Geol 237, 211-232.
514 Bartley, J.K., Semikhatov, M.A., Kaufman, A.J., Knoll, A.H., Pope, M.C., Jacobsen, S.B., 2001. Global
515 events across the Mesoproterozoic-Neoproterozoic boundary: C and Sr isotopic evidence from
516 Siberia. Precambrian Res 111, 165-202.

517 Bekker, A., Kaufman, A.J., Karhu, J.A., Eriksson, K.A., 2005. Evidence for Paleoproterozoic cap
518 carbonates in North America. Precambrian Research 137, 167-206.
519 Birck, J.L, Roy Barman, M., Capmas, F., 1997. Re-Os isotopic measurements at the femtomole level in
520 natural samples. Geostandards Newsletter 21, 19-27.
521 Brody, K.B., Kaufman, A.J., Eigenbrode, J.L., Cody, G.D., 2004. Biomarker geochemistry of a post-
522 glacial Neoproterozoic succession in Brazil, Geological Society of America Annual Meeting
523 (Abstract), Denver, CO.
524 Buick, R., Marais, D.J.D., Knoll, A.H., 1995. Stable Isotopic Compositions of Carbonates from the
525 Mesoproterozoic Bangemall Group, Northwestern Australia. Chem Geol 123, 153-171.
526 Canfield, D.E., 1998. A new model for Proterozoic ocean chemistry. Nature 396, 450-453.
527 Canfield, D.E., Raiswell, R., Westrich, J.T., Reaves, C.M., Berner, R.A., 1986. The Use of Chromium
528 Reduction in the Analysis of Reduced Inorganic Sulfur in Sediments and Shales. Chem Geol 54,
529 149-155.
530 Canfield, D.E., Raiswell, R., Bottrell, S., 1992. The reactivity of sedimentary iron minerals toward
531 sulfide. Am J Sci 292, 659-683.
532 Cloud, P., Dardenne, M.A., 1973. Proterozoic age of the Bambui Group in Brazil. Geol Soc Am Bull 84,
533 1673-1676.
534 Cohen, A.S., Coe, A.L., Bartlett, J.M., Hawkesworth, C.J., 1999. Precise Re-Os ages of organic-rich
535 mudrocks and the Os isotope composition of Jurassic seawater. Earth Planet Sc Lett 167, 159-
536 173.
537 Cohen, A.S., Waters, F.G., 1996. Separation of osmium from geological materials by solvent extraction
538 for analysis by thermal ionization mass spectrometry. Analytica Chimica Acta 332, 269-275.
539 Corsetti, F.A., Olcott, A.N., Bakermans, C., 2006. The biotic response to Neoproterozoic snowball Earth.
540 Palaeogeogr Palaeocl Palaeoeco 232, 114-130.
541 Creaser, R.A., Sannigrahi, P., Chacko, T., Selby, D., 2002. Further evaluation of the Re-Os
542 geochronometer in organic-rich sedimentary rocks: A test of hydrocarbon maturation effects in

the Exshaw Formation, Western Canada Sedimentary Basin. Geochim Cosmochim Ac 66, 3441-3452.

Dardenne, M.A., 1978. Zonação tectônica na borda ocidental do Cráton São Francisco. Anais Congresso Brasileiro de Geologia, Sociedade Brasileira de Geologia, Recife, v. 1, pp. 299-308.

Dardenne, M.A., 2000. The Brasilia Fold Belt, in: Cordani, U.G., Milani, E.J., Filho, A.T., Campos, D.A. (Eds.), The Brasilia Fold Belt in Tectonic Evolution of South America. 31st International Geological Congress, Rio de Janeiro, pp. 231-263.

Dardenne, M.A., 2001. Lithostratrigraphic sedimentary sequences of the Vazante Group, in: IGCP 450 Proterozoic Sediment-Hosted Base Metal Deposits of Western Gondwana (abstract), Belo Horizonte, pp. 48-50.

Dardenne, M.A., Campos Neto, M.C., 1976. Geologia da regiao de Lagamar, Minas Gerais, Congresso Brasileiro de Geologia, 29, Ouro Preto, resumos, pp. 17.

Derry, L.A., Kaufman, A.J., Jacobsen, S.B., 1992. Sedimentary cycling and environmental-change in the Late Proterozoic - evidence from stable and radiogenic isotopes. Geochim Cosmochim Ac 56, 1317-1329.

Gilleaudeau, G.J., Kah, L.C. (2013) Carbon isotope records in a Mesoproterozoic epicratonic sea: Carbon cycling in a low-oxygen world. Precambrian Res 228, 85-101.

Halverson, G.P., Wade, B.P., Hurtgen, M.T., Barovich, K.M., 2010. Neoproterozoic chemostratigraphy. Precambrian Res 182, 337-350.

Hannah, J.L., Bekker, A., Stein, H.J., Markey, R.J., Holland, H.D., 2004. Primitive Os and 2316 Ma age for marine shale: implications for Paleoproterozoic glacial events and the rise of atmospheric oxygen. Earth Planet Sc Lett 225, 43-52.

Harland, W.B., and Bidgood, D.E.T., 1959. Palaeomagnetism in some Norwegian sparagmites and the late Pre-Cambrian ice age. Nature 184, 1860-1862.

Hoffman, P.F., Kaufman, A.J., Halverson, G.P., Schrag, D.P., 1998. A Neoproterozoic snowball earth. Science 281, 1342-1346.

569 Jaffe, L.A., Peucker-Ehrenbrink, B., Petsch, S.T., 2002. Mobility of rhenium, platinum group elements
570 and organic carbon during black shale weathering. Earth Planet Sc Lett 198, 339-353.
571 Johnston, D.T., Macdonald, F.A., Gill, B.C., Hoffman, P.F., and Schrag, D.P., 2012. Uncovering the
572 Neoproterozoic carbon cycle. Nature 483, 320-324.
573 Kah, L.C., Bartley, J.K., Teal, D.A., 2012. Chemostratigraphy of the Late Mesoproterozoic Atar Group,
574 Taoudeni Basin, Mauritania: Muted isotopic variability, facies correlation, and global isotopic
575 trends. Precambrian Res 200, 82-103.
576 Kah, L.C., Lyons, T.W., Chesley, J.T., 2001. Geochemistry of a 1.2 Ga carbonate-evaporite succession,
577 northern Baffin and Bylot Islands: implications for Mesoproterozoic marine evolution.
578 Precambrian Res 111, 203-234.
579 Kah, L.C., Lyons, T.W., Frank, T.D., 2004. Low marine sulphate and protracted oxygenation of the
580 proterozoic biosphere. Nature 431, 834-838.
581 Kah, L.C., Sherman, A.G., Narbonne, G.M., Knoll, A.H., Kaufman, A.J., 1999. delta C-13 stratigraphy of
582 the Proterozoic Bylot Supergroup, Baffin Island, Canada: implications for regional
583 lithostratigraphic correlations. Can J Earth Sci 36, 313-332.
584 Kaufman, A.J., Hayes, J.M., Knoll, A.H., Germs, G.J.B., 1991. Isotopic compositions of carbonates and
585 organic-carbon from upper Proterozoic successions in Namibia-Stratigraphic variation and the
586 effects of diagenesis and metamorphism. Precambrian Res 49, 301-327.
587 Kaufman, A.J., Knoll, A.H., 1995. Neoproterozoic Variations in the C-Isotopic Composition of Seawater
588 - Stratigraphic and Biogeochemical Implications. Precambrian Res 73, 27-49.
589 Kaufman, A.J., Knoll, A.H., Narbonne, G.M., 1997. Isotopes, ice ages, and terminal Proterozoic earth
590 history. P Natl Acad Sci USA 94, 6600-6605.
591 Kendall, B., Creaser, R.A., Selby, D., 2006. Re-Os geochronology of postglacial black shales in
592 Australia: Constraints on the timing of "Sturtian" glaciation. Geology 34, 729-732.

593 Kendall, B., Creaser, R.A., Ross, G.M., Selby, D., 2004. Constraints on the timing of Marinoan
594 "Snowball Earth" glaciation by Re-187-Os-187 dating of a Neoproterozoic, post-glacial black
595 shale in Western Canada. Earth Planet Sc Lett 222, 729-740.
596 Kendall, B., Creaser, R.A., Gordon, G.W., Anbar, A.D., 2009. Re-Os and Mo isotope systematics of
597 black shales from the Middle Proterozoic Velkerri and Wollogorang Formations, McArthur
598 Basin, northern Australia. Geochim Cosmochim Ac 73, 2534-2558.
599 Kennedy, M.J., 1996. Stratigraphy, sedimentology, and isotopic geochemistry of Australian
600 Neoproterozoic postglacial cap dolostones: Deglaciation, delta C-13 excursions, and carbonate
601 precipitation. Journal of Sedimentary Research 66, 1050-1064.
602 Kennedy, M.J., Runnegar, B., Prave, A.R., Hoffmann, K.H., Arthur, M.A., 1998. Two or four
603 Neoproterozoic glaciations? Geology 26, 1059-1063.
604 Kirschvink, J.W., 1992. Late Proterozoic low-latitude global glaciations: the Snowball Earth, in: Schopf,
605 J.W., Klein, C. (Eds.), The Proterozoic Biosphere. Cambridge University Press, Cambridge, pp.
606 51-52.
607 Knoll, A.H., Hayes, J.M., Kaufman, A.J., Swett, K., Lambert, I.B., 1986. Secular Variation in Carbon
608 Isotope Ratios from Upper Proterozoic Successions of Svalbard and East Greenland. Nature 321,
609 832-838.
610 Knoll, A.H., Kaufman, A.J., Semikhatov, M.A., 1995. The carbon-isotopic composition of Proterozoic
611 carbonates: Riphean successions from northwestern Siberia (Anabar Massif, Turukhansk uplift).
612 Am J Sci 295, 823-850.
613 Levasseur, S., Birck, J.-L., Allègre, C.J., 1999. The osmium riverine flux and the oceanic mass balance of
614 osmium. Earth Planet Sci Lett 174, 7-23.
615 Marshall, A.O., Corsetti, F.A., Sessions, A.L., Marshall, C.P., 2009. Raman spectroscopy and biomarker
616 analysis reveal multiple carbon inputs to a Precambrian glacial sediment. Organic Geochemistry
617 40, 1115-1123.

618 Misi, A., Azmy, K., Kaufman, A.J., Oliveira, T.F., Pinho, J.M., Sanches, A.L., 2010. Metallogenic and
619 phosphogenic events in the intracratonic and passive-margin Proterozoic basins of the São
620 Francisco Craton: The Bambuí/Una and Vazante Groups. VII South American Symposium on
621 Isotope Geology, Brasilia, DF. Extended Abstracts.
622 Misi, A., Azmy, K., Kaufman, A.J., Oiveira, T. F., Pinho, J. M., Sanches, A.L., 2011. High resolution
623 chemostratigraphy and Re-Os ages of organic shales of the Vazante Group (Minas Gerais,
624 Brazil): Implications for mineral exploration modelling. In: XIV Congreso Latino Americano de
625 Geologia, Medellin. Memorias, v. 1. p. 410-411.
626 Misi, A., Iyer, S.S.S., Coelho, C.E.S., Tassinari, C.C.G., Franca-Rocha, W.J.S., Cunha, I.D., Gomes,
627 A.S.R., de Oliveira, T.F., Teixeira, J.B.G., Filho, V.M.C., 2005. Sediment hosted lead-zinc
628 deposits of the Neoproterozoic Bambui Group and correlative sequences, Sao Francisco Craton,
629 Brazil: A review and a possible metallogenic evolution model. Ore Geol Rev 26, 263-304.
630 Misi, A., Kaufman, A.J., Veizer, J., Powis, K., Azmy, K., Boggiani, P.C., Gaucher, C., Teixeira, J.B.G.,
631 Sanches, A.L., Iyer, S.S.S., 2007. Chemostratigraphic correlation of neoproterozoic successions
632 in South America. Chem Geol 237, 143-167.
633 Olcott, A.N., Sessions, A.L., Corsetti, F.A., Kaufman, A.J., de Oliviera, T.F., 2005. Biomarker evidence
634 for photosynthesis during Neoproterozoic glaciation. Science 310, 471-474.
635 Pimentel, M.M., Dardenne, M.A., Fuck, R.A., Viana, M.G., Junges, S.L., Fischel, D.P., Seer, H.J.,
636 Dantas, E.L., 2001. Nd isotopes and the provenance of detrital sediments of the Neoproterozoic
637 Brasilia Belt, central Brazil. J S Am Earth Sci 14, 571-585.
638 Pinho, J.M.M., Dardenne, M.A., 1994. Caracterização da Falha de Lagamar, NW de Minas Gerais.
639 Abstracts, 38th Brazilian Geological Congress, Sociedade Brasileira de Geologia, Camboriú, SC
640 p.246-247.
641 Poulton, S.W., Canfield, D.E., 2005. Development of a sequential extraction procedure for iron:
642 implications for iron partitioning in continentally derived particulates. Chem Geol 214, 209-221.

643 Poulton, S.W., Raiswell, R., 2002. The low-temperature geochemical cycle of iron: From continental
644 fluxes to marine sediment deposition. Am J Sci 302, 774-805.
645 Poulton, S.W., Canfield, D.E., 2011. Ferruginous conditions: A dominant feature of the ocean through
646 Earth's history. Elements 7, 107-112.
647 Poulton, S.W., Krom, M.D., Raiswell, R., 2004a. A revised scheme for the reactivity of iron
648 (oxyhydr)oxide minerals towards dissolved sulfide. Geochim Cosmochim Acta 68, 3703-3715.
649 Poulton, S.W., Fralick, P.W., Canfield, D.E., 2004b. The transition to a sulphidic ocean ~1.84 billion
650 years ago. Nature 431, 173-177.
651 Prave, A.R., Fallick, A.E., Thomas, C.W., Graham, C.M., 2009. A composite C-isotope profile for the
652 Neoproterozoic Dalradian Supergroup of Scotland and Ireland. J Geol Soc London 166, 845-
653 857.
654 Raiswell, R. Canfield, D.E., 1998. Sources of iron for pyrite formation in modern sediments. Am J Sci
655 298, 219-245.
656 Ravizza, G., Turekian, K.K., 1989. Application of the Re-187-Os-187 System to Black Shale
657 Geochronometry. Geochimica Et Cosmochimica Acta 53, 3257-3262.
658 Rodrigues, J.B., Pimentel, M.M., Buhn, B., Matteini, M., Dardenne, M.A., Alvarenga, C.J.S., Armstrong,
659 R.A., 2012. Provenance of the Vazante Group: New U-Pb, Sm-Nd, Lu-Hf isotopic data and
660 implications for the tectonic evolution of the Neoproterozoic Brasilia Belt. Gondwana Res 21,
661 439-450.
662 Rooney, A.D., Selby, D., Houzay, J.P., Renne, P.R., 2010. Re-Os geochronology of a Mesoproterozoic
663 sedimentary succession, Taoudeni basin, Mauritania: Implications for basin-wide correlations
664 and Re-Os organic-rich sediments systematics. Earth Planet Sc Lett 289, 486-496.
665 Santos, R.V., de Alvarenga, C.J.S., Dardenne, M.A., Sial, A.N., Ferreira, V.P., 2000. Carbon and oxygen
666 isotope profiles across Meso-Neoproterozoic limestones from central Brazil: Bambui and
667 Paranoa groups. Precambrian Res 104, 107-122.

668 Schrag, D.P., Berner, R.A., Hoffman, P.F., and Halverson, G.P., 2002. On the initiation of a snowball
669 Earth. Geochemistry Geophysics Geosystems 3, 6, 1-21.
670 Selby, D., Creaser, R.A., 2003. Re-Os geochronology of organic rich sediments: an evaluation of organic
671 matter analysis methods. Chem Geol 200, 225-240.
672 Shirey, S.B., Walker, R.J., 1995. Carius Tube Digestion for Low-Blank Rhenium-Osmium Analysis. Anal
673 Chem 67, 2136-2141.
674 Tohver, E., D'Agrella, M.S., Trindade, R.I.F., 2006. Paleomagnetic record of Africa and South America
675 for the 1200-500 Ma interval, and evaluation of Rodinia and Gondwana assemblies.
676 Precambrian Res 147, 193-222.
677 Walker, R.J., Horan, M.F., Morgan, J.W., Becker, H., Grossman, J.N., Rubin, A.E., 2002a. Comparative
678 ^{187}Re-^{187}Os systematics of chondrites: implications regarding early solar system processes.
679 Geochim Cosmochim Acta 66, 4187-4201.
680 Walker, R.J., Prichard, H.M., Ishiwatari, A., Pimentel, M., 2002b. The osmium isotopic composition of
681 the convecting upper mantle deduced from ophiolite chromites. Geochim Cosmochim Acta 66,
682 329-345.
683 Walter, M.R., Veevers, J.J., Calver, C.R., Gorjan, P., Hill, A.C., 2000. Dating the 840-544 Ma
684 Neoproterozoic interval by isotopes of strontium, carbon, and sulfur in seawater, and some
685 interpretative models. Precambrian Research 100, 371-433.
686 Weil, A.B., Van der Voo, R., Mac Niocaill, C., Meert, J.G., 1998. The Proterozoic supercontinent
687 Rodinia: paleomagnetically derived reconstructions for 1100 to 800 Ma. Earth Planet Sc Lett
688 154, 13-24.
689

690 **Captions**

691 Figure 1: Geologic map of study area. The Vazante Group is elongated north to south within Brazil with
692 ┼ indicating the approximate location of the drill cores examined here. Modified from Babinski et al.
693 (2005).

694

695 Figure 2: Generalized stratigraphy of the Vazante Group with formation and member names highlighting
696 sub-glacial valleys and post-glacial fill, the newly discovered reverse fault and geochronometric
697 constraints discussed in the text. Modified after Dardenne (2000) with generalized C-isotope trends from
698 Azmy et al. (2001; 2006). No vertical scale implied.

699

700 Figure 3: Photographs of A. carbonate ice-rafted debris in the organic-rich post-glacial shale of the Morro
701 do Calcário Formation in drill core MASW-01; B. faceted cobble in silicified shale matrix of the Morro
702 do Calcário Formation near Paracatu, MG, Brazil; C. *Conophyton* stromatolites from the basal Lagamar
703 Formation above the thrust fault; D. phosphorite and high-Sr limestone from the Rocinha Formation
704 located below the thrust fault and west of the Vazante mine; E. thrust fault trace with brown to mauve
705 sandy mylonite to the left and bedded purple shale and siltstone of the upper Rocinha Formation to the
706 right; F. Close up of clay and quartz-rich mylonite at thrust fault contact.

707

708 Figure 4: Re-Os isochrons for: A. Serra do Garrote Formation samples from drill core 134-86; B. Morro
709 do Calcário Formation samples from drill core 42-88 and 134-86; C. Morro do Calcário Formation
710 samples taken only from drill core 134-86.

711

712 Figure 5: Time-series elemental and stable isotope compositions of the Serra do Garrote, Morro do
713 Calcário and Lapa Formations (shale intervals only) in the Mesoproterozoic Vazante Group, drill core
714 134-86 (data available in Table 2), where TOC = total organic carbon.

715

Figure 6: Time-series elemental and stable isotope compositions of the Morro do Calcário Formation shale interval in the Mesoproterozoic Vazante Group, drill core 42-88 (data available in Tables 2 and 3), where TOC = total organic carbon and S = sulfide-sulfur. Iron speciation data allows identification of deposition from an oxic, anoxic non-sulfidic or euxinic (free sulfide) water column. FeHR = highly reactive iron; FeT = total iron; FeS = pyrite iron. Euxinic conditions are interpreted from FeHR/FeT > 0.38 and FeS/FeHR > ~0.7; anoxic non-sulfidic conditions are recognized from FeHR/FeT > 0.38 and FeS/FeHR < ~0.7; oxic conditions are demonstrated by FeHR/FeT < 0.22. Dashed lines are presented at these threshold values. For all data points, the uncertainty on the measurement is smaller than the symbol.

Table 1: Re and Os abundance and isotope data for black shale intervals in the Serra do Garrote, Morro do Calcário and Lapa Formations. Os_i = initial $^{187}Os/^{188}Os$ ratio back-calculated using the isochron age in Figure 4.

Table 2: Time-series total organic carbon (TOC) abundances in weight percent; carbon isotopic composition of the organic carbon ($\delta^{13}C$); sulfur isotopic composition of the sulfide sulfur ($\delta^{34}S$); and sulfide sulfur abundance in weight percent (S) of the Serra do Garrote, Morro do Calcário and Lapa Formations in drill core 134-86 as well as the Morro do Calcário Formation of drill core 42-88. Uncertainties do not exceed: TOC and S ± 10% of value; $\delta^{13}C$ ± 0.15‰; $\delta^{34}S$ ± 0.35‰. nd = not detected.

Table 3: Results from the analysis of the Morro do Calcário Formation shale interval in the Mesoproterozoic Vazante Group, drill core 42-88. Iron speciation analyses: All concentrations are in weight % (nd = not detected). FeT = total iron; Fecarb = carbonate iron; Fox = oxide iron; Femag = magnetite iron; Fe-AVS = acid volatile sulfide iron; Fepy = pyrite iron; FeHR = highly reactive iron; Fe-S = Fe-AVS + Fepy.

Fig. 1

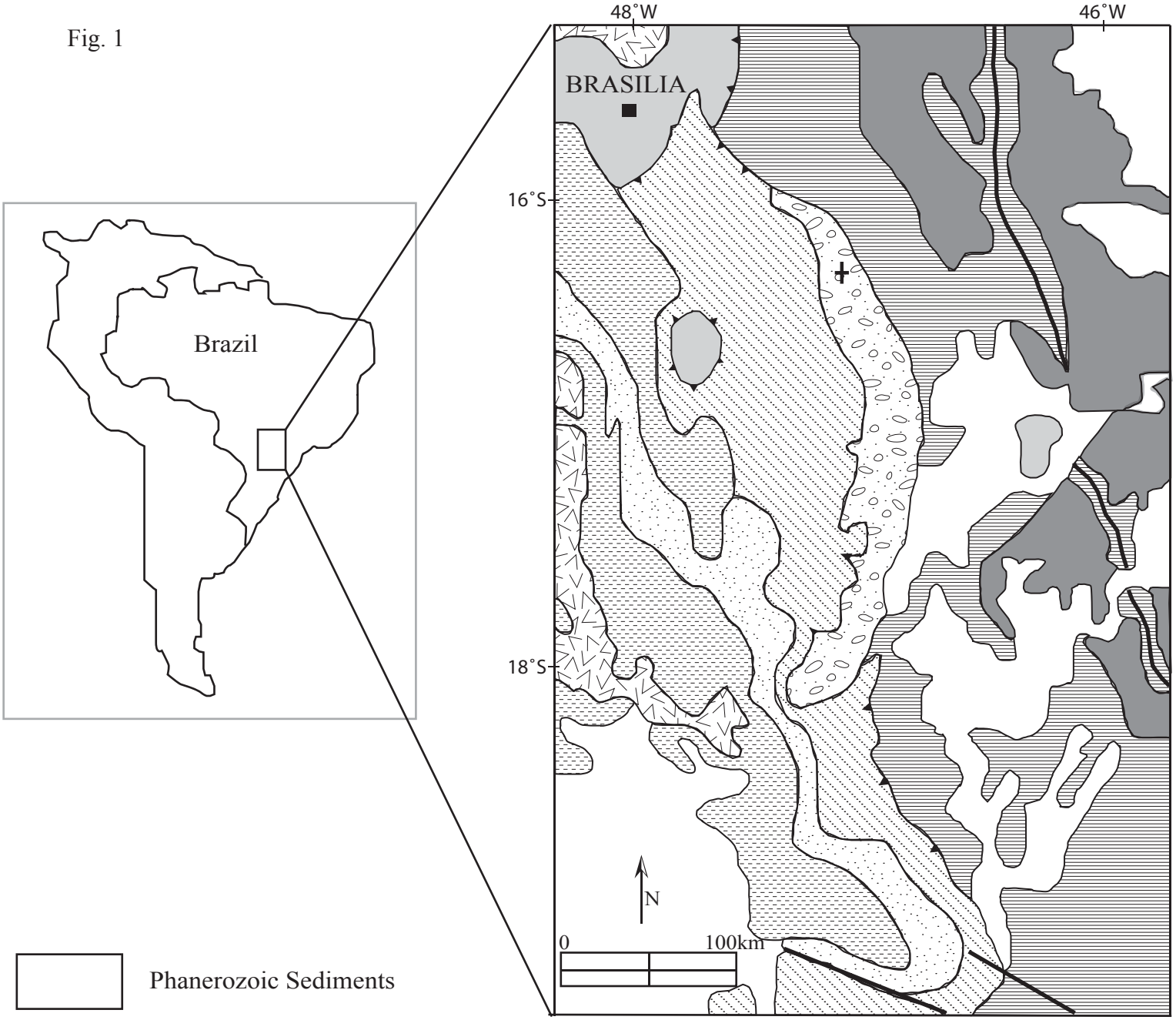
48°W
46°W
BRASILIA
16°S
18°S
Brazil
N
0
100km
Phanerozoic Sediments
Bambuí Group
Três Marias Fm.
Paraopeba Subgroup
Brasília Fold Belt
Ibía Fm.
Araxá Group
Granulites
Vazante Group
Paranoá Group
Canastra Group

Fig. 2

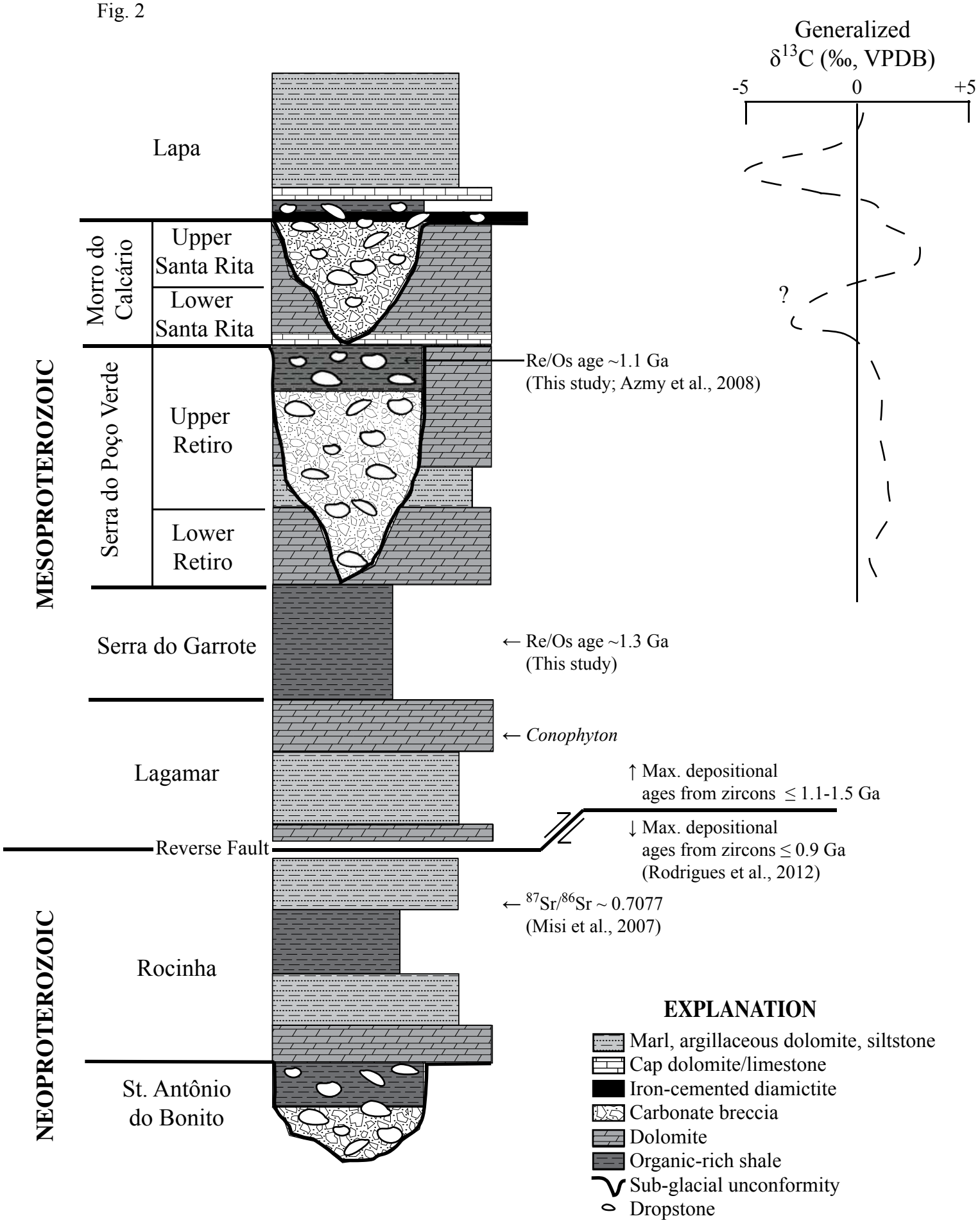
Generalized
$\delta^{13}C$ (‰, VPDB)
-5
0
+5
?
MESOPROTEROZOIC
NEOPROTEROZOIC
Lapa
Morro do Calcário
Upper Santa Rita
Lower Santa Rita
Serra do Poço Verde
Upper Retiro
Lower Retiro
Serra do Garrote
Lagamar
Rocinha
St. Antônio do Bonito
Reverse Fault
Re/Os age ~1.1 Ga
(This study; Azmy et al., 2008)
← Re/Os age ~1.3 Ga
(This study)
← *Conophyton*
↑ Max. depositional ages from zircons ≤ 1.1-1.5 Ga
↓ Max. depositional ages from zircons ≤ 0.9 Ga
(Rodrigues et al., 2012)
← $^{87}Sr/^{86}Sr$ ~ 0.7077
(Misi et al., 2007)
EXPLANATION
Marl, argillaceous dolomite, siltstone
Cap dolomite/limestone
Iron-cemented diamictite
Carbonate breccia
Dolomite
Organic-rich shale
Sub-glacial unconformity
Dropstone

Fig. 3

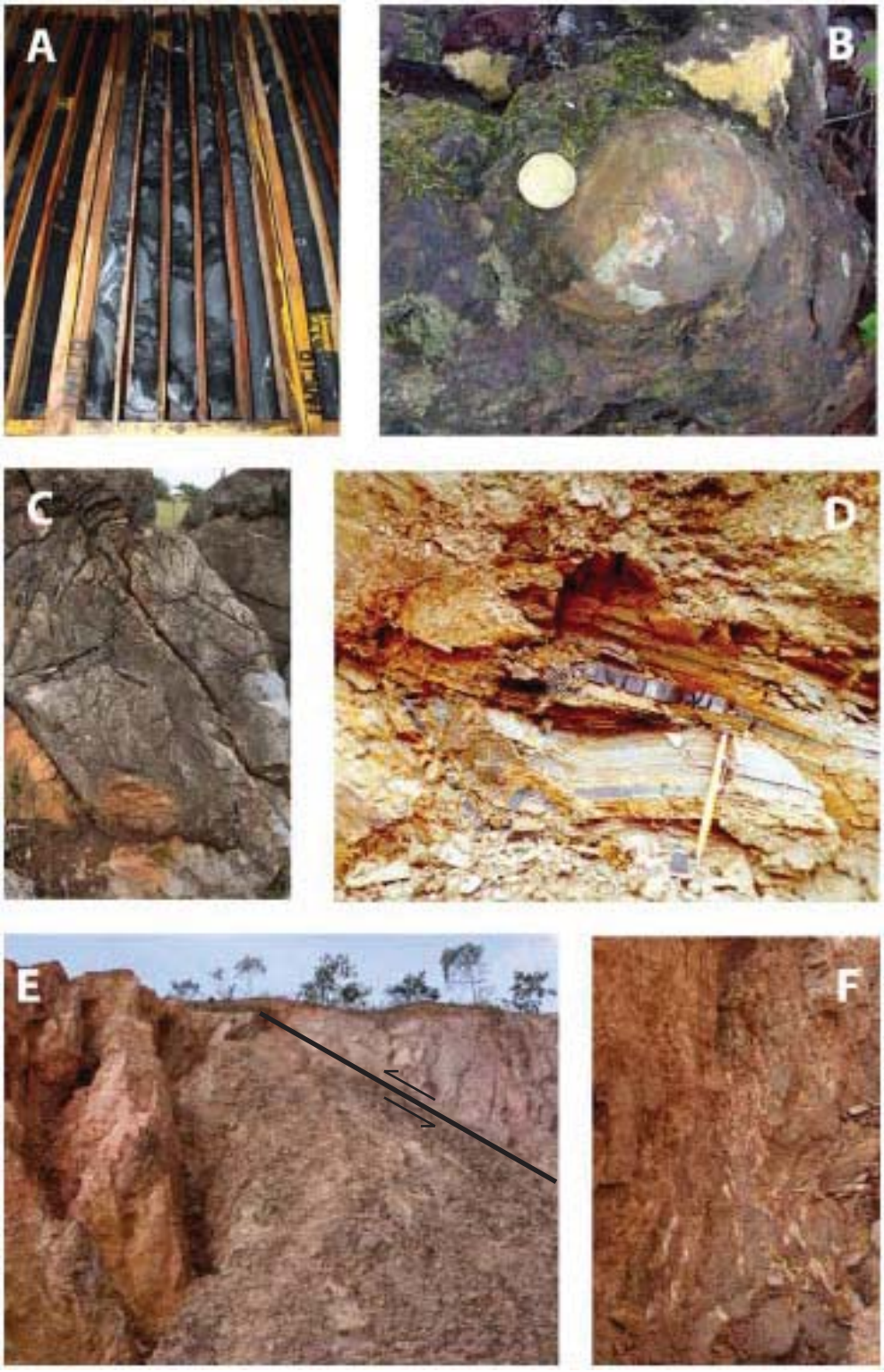

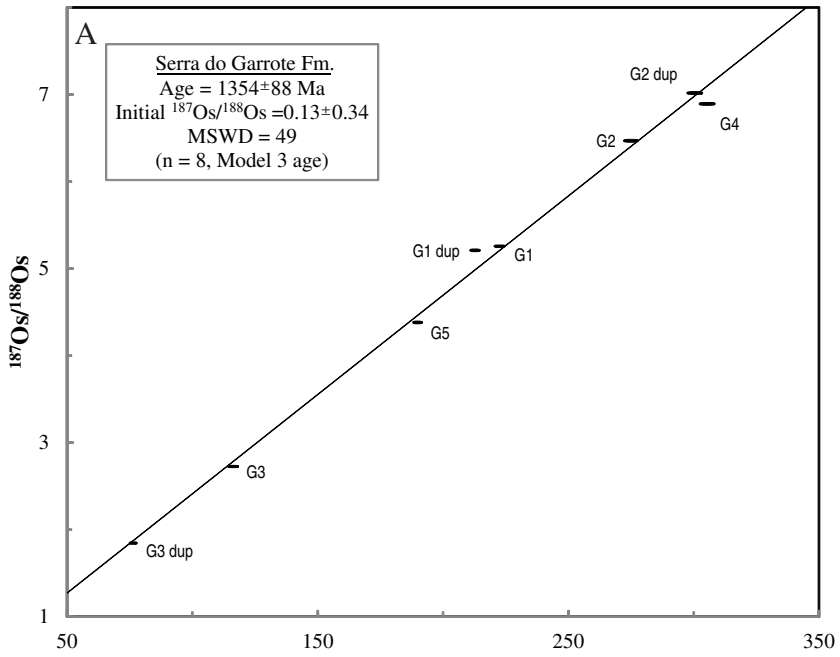
A
Serra do Garrote Fm.
Age = 1354±88 Ma
Initial 187Os/188Os =0.13±0.34
MSWD = 49
(n = 8, Model 3 age)
G2 dup
G4
G2
G1 dup
G1
G5
G3
G3 dup
187Os/188Os
1
3
5
7
50
150
250
350

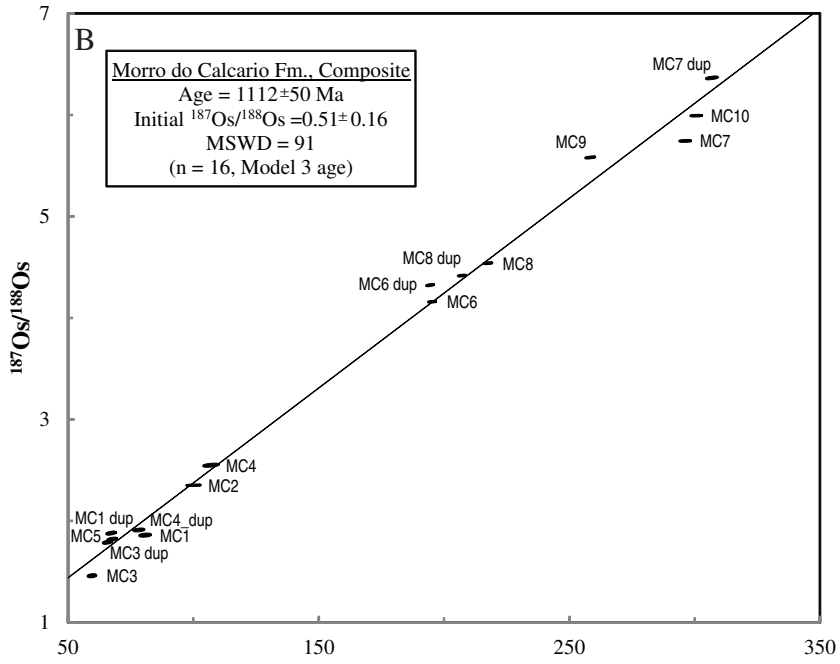
B
Morro do Calcario Fm., Composite
Age = 1112±50 Ma
Initial 187Os/188Os =0.51± 0.16
MSWD = 91
(n = 16, Model 3 age)
MC7 dup
MC10
MC9
MC7
MC8 dup
MC8
MC6 dup
MC6
MC4
MC2
MC1 dup
MC4_dup
MC5
MC1
MC3 dup
MC3
187Os/188Os
1
3
5
7
50
150
250
350

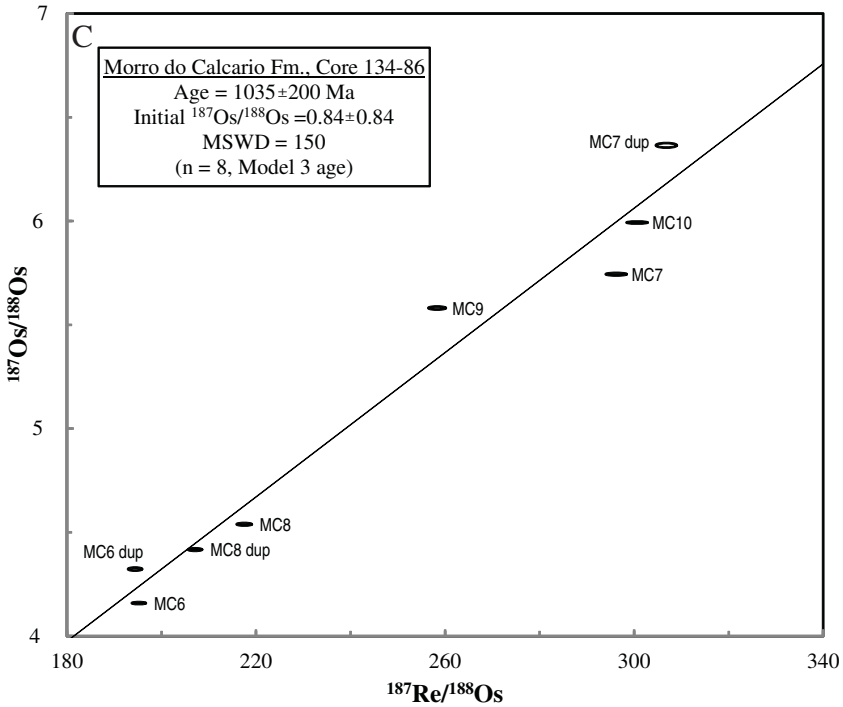
C
Morro do Calcario Fm., Core 134-86
Age = 1035±200 Ma
Initial 187Os/188Os =0.84±0.84
MSWD = 150
(n = 8, Model 3 age)
MC7 dup
MC10
MC7
MC9
MC8
MC8 dup
MC6 dup
MC6
187Os/188Os
4
5
6
7
180
220
260
300
340
187Re/188Os

Fig. 5

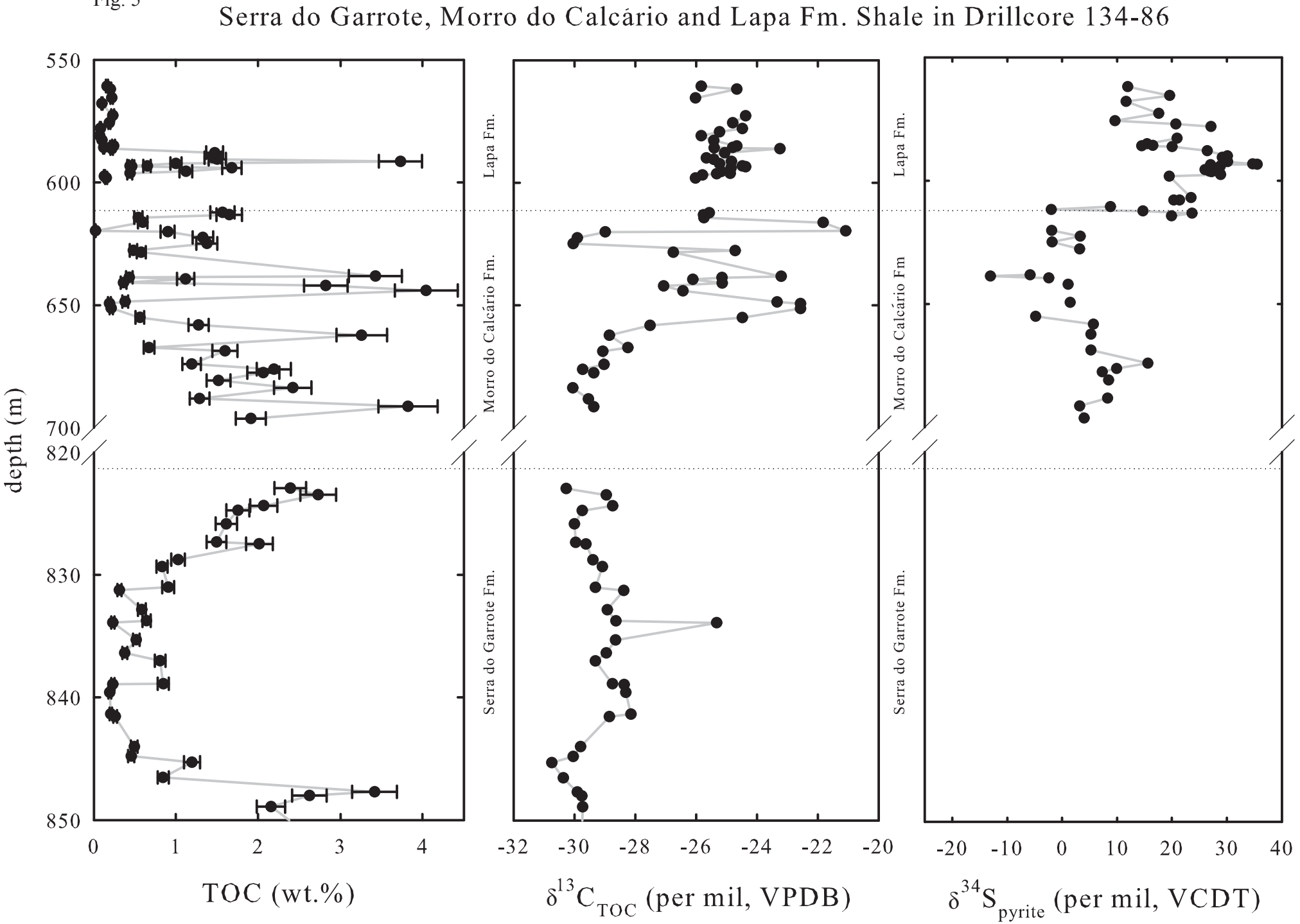
Serra do Garrote, Morro do Calcário and Lapa Fm. Shale in Drillcore 134-86
depth (m)
550
600
650
700
820
830
840
850
Lapa Fm.
Morro do Calcário Fm.
Serra do Garrote Fm.
0
1
2
3
4
TOC (wt.%)
-32
-30
-28
-26
-24
-22
-20
δ13CTOC (per mil, VPDB)
-20
-10
0
10
20
30
40
δ34Spyrite (per mil, VCDT)

Fig. 6

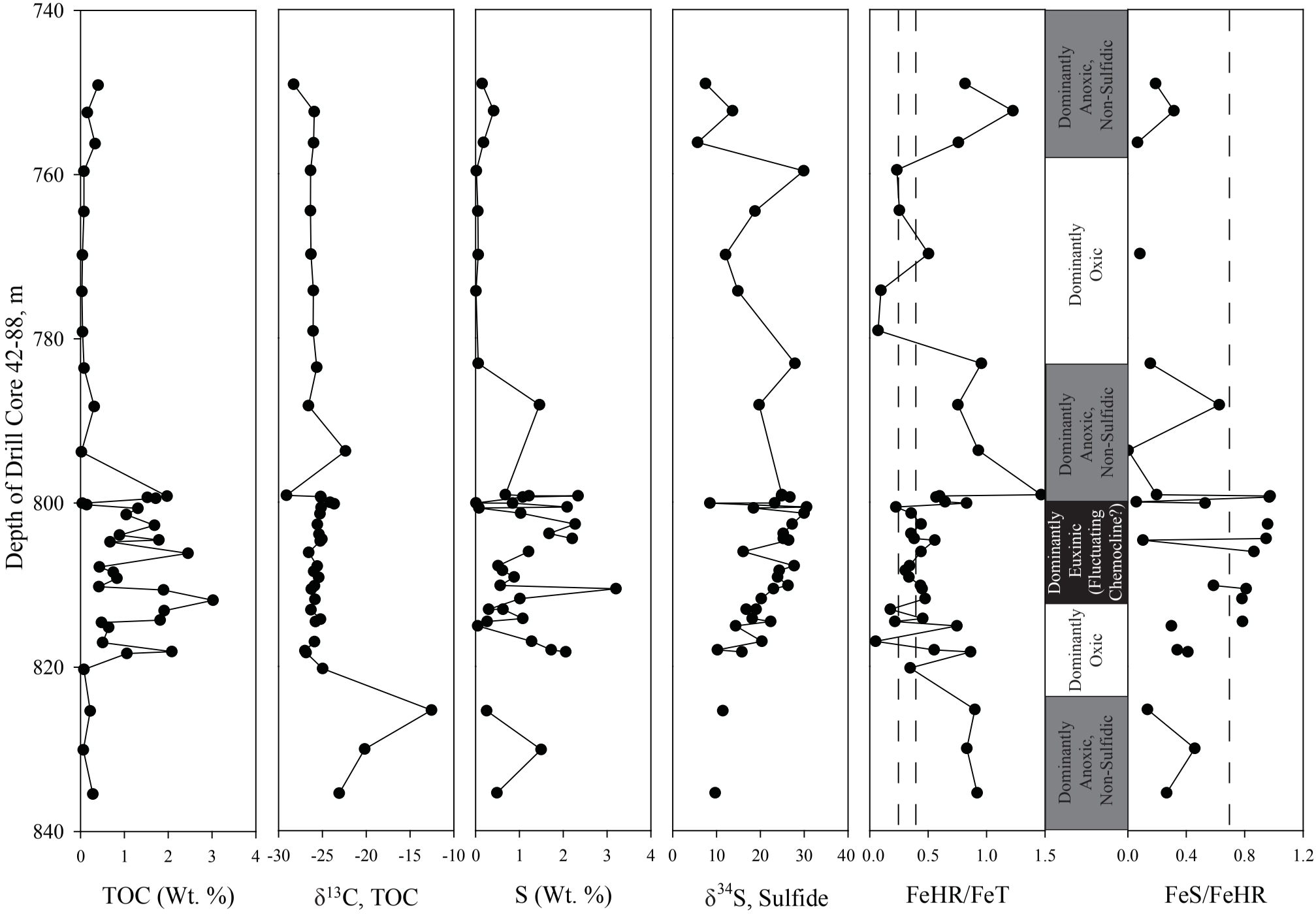
Depth of Drill Core 42-88, m
740
760
780
800
820
840
TOC (Wt. %)
0 1 2 3 4
δ13C, TOC
-30 -25 -20 -15 -10
S (Wt. %)
0 1 2 3 4
δ34S, Sulfide
0 10 20 30 40
FeHR/FeT
0.0 0.5 1.0 1.5
FeS/FeHR
0.0 0.4 0.8 1.2
Dominantly Anoxic, Non-Sulfidic
Dominantly Oxic
Dominantly Anoxic, Non-Sulfidic
Dominantly Euxinic (Fluctuating Chemocline?)
Dominantly Oxic
Dominantly Anoxic, Non-Sulfidic

Table 1

	Sample	Drill Hole	Core Depth	Re (ppb)	Os (ppt)	^{187}Re / ^{188}Os	^{187}Os / ^{188}Os	Os_i
Lapa Fm.	L1	134-86	587.84	0.322 ± 0.008	35.0 ± 0.4	53.34 ± 1.19	1.709 ± 0.003	N/A
	L2	134-86	589.90	0.288 ± 0.008	33.4 ± 0.4	50.73 ± 1.53	1.838 ± 0.007	N/A
	L3	134-86	590.50	0.138 ± 0.008	26.1 ± 0.4	30.4 ± 1.8	1.59 ± 0.01	N/A
	L4	134-86	591.34	0.366 ± 0.008	52.3 ± 0.5	39.05 ± 0.92	1.358 ± 0.006	N/A
Morro do Calcário Fm.	MC1	42-88	803.89	0.435 ± 0.009	31.6 ± 0.1	80.7 ± 1.8	1.86 ± 0.01	0.33
	MC1_dup	42-88	803.89	0.360 ± 0.007	31.5 ± 0.1	67.2 ± 1.5	1.88 ± 0.01	0.6
	MC2	42-88	804.00	0.690 ± 0.014	42.5 ± 0.1	100.0 ± 2.2	2.352 ± 0.003	0.46
	MC3	42-88	804.43	0.334 ± 0.007	31.6 ± 0.1	59.5 ± 1.3	1.46 ± 0.01	0.34
	MC3_dup	42-88	804.43	0.303 ± 0.006	26.9 ± 0.1	65.7 ± 1.4	1.79 ± 0.01	0.54
	MC4	42-88	804.48	0.858 ± 0.017	50.5 ± 0.2	107.0 ± 2.4	2.549 ± 0.01	0.53
	MC4_dup	42-88	804.48	0.831 ± 0.017	62.9 ± 0.2	78.2 ± 1.7	1.911 ± 0.009	0.44
	MC5	42-88	804.50	0.387 ± 0.008	33.5 ± 0.1	67.6 ± 1.5	1.82 ± 0.01	0.54
	MC6	134-86	676.05	3.498 ± 0.014	131.1 ± 0.4	195.2 ± 1.2	4.159 ± 0.004	0.46
	MC6_dup	134-86	676.05	3.485 ± 0.014	132.9 ± 0.4	194.4 ± 1.2	4.323 ± 0.006	0.64
	MC7	134-86	677.40	8.702 ± 0.035	244.4 ± 0.7	296.2 ± 1.8	5.744 ± 0.005	0.21
	MC7_dup	134-86	677.40	8.030 ± 0.032	227.7 ± 0.7	306.8 ± 1.8	6.365 ± 0.009	0.63
	MC8	134-86	680.78	6.137 ± 0.025	213.5 ± 0.6	217.5 ± 1.3	4.539 ± 0.005	0.47
	MC8_dup	134-86	680.78	5.871 ± 0.023	212.3 ± 0.6	207.1 ± 1.2	4.417 ± 0.005	0.54
	MC9	134-86	683.60	4.070 ± 0.016	129.0 ± 0.4	258.3 ± 1.5	5.581 ± 0.006	0.68
	MC10	134-86	691.23	6.570 ± 0.026	184.9 ± 0.6	300.6 ± 1.8	5.993 ± 0.004	0.35
Serra do Garrote Fm.	G1	134-86	824.37	16.02 ± 0.07	578.7 ± 1.2	222.5 ± 1.5	5.257 ± 0.003	0.19
	G1_dup	134-86	824.37	15.63 ± 0.07	588.7 ± 1.2	212.7 ± 1.4	5.209 ± 0.005	0.19
	G2	134-86	824.42	11.56 ± 0.06	370.1 ± 0.7	274.9 ± 2.1	6.468 ± 0.006	0.20
	G2_dup	134-86	824.42	11.72 ± 0.06	356.8 ± 0.7	300.4 ± 2.3	7.017 ± 0.006	0.17
	G3	134-86	824.76	1.093 ± 0.012	60.6 ± 0.1	116.2 ± 1.5	2.724 ± 0.003	0.07
	G3_dup	134-86	824.76	1.038 ± 0.012	80.2 ± 0.2	76.31 ± 1.00	1.844 ± 0.002	0.10
	G4	134-86	825.83	11.97 ± 0.07	355.4 ± 0.7	305.3 ± 2.3	6.892 ± 0.006	-0.07
	G5	134-86	825.86	5.650 ± 0.028	223.5 ± 0.4	189.8 ± 1.3	4.38 ± 0.005	0.06

Table 2

	Depth (m) Core 134-86	TOC (Wt. %)	$\delta^{13}C$, TOC	$\delta^{34}S$, Sulfide		Depth (m) Core 134-86	TOC (Wt. %)	$\delta^{13}C$, TOC		Depth (m) Core 42-88	TOC (Wt. %)	$\delta^{13}C$, TOC	S (Wt. %)	$\delta^{34}S$, Sulfide
Lapa Fm.	560.70	0.161	-25.83	nd	Serra do Garrote Fm.	822.93	2.39	-30.27	Morro do Calcário Fm.	749.03	0.404	-28.3	0.15	7.49
	561.82	0.2	-24.66	11.91		823.45	2.73	-28.95		752.35	0.156	-25.9	0.42	13.7
	565.40	0.22	-26.02	19.58		824.35	2.07	-28.74		756.20	0.333	-26.0	0.18	5.69
	567.83	0.1	--	11.67		824.73	1.75	-29.74		759.55	0.0797	-26.3	0.017	29.9
	572.64	0.23	-24.37	17.59		825.83	1.61	-30.00		764.47	0.0788	-26.4	0.052	18.8
	575.60	0.19	-24.80	9.62		827.32	1.49	-29.96		769.75	0.0440	-26.3	0.061	12.1
	576.93	nd	nd	20.69		827.47	2.01	-29.62		774.20	0.0336	-26.0	0.0087	14.9
	577.92	0.08	-24.48	27.09		828.75	1.03	-29.39		779.10	--	--	--	--
	579.27	--	-25.23	nd		829.32	0.832	-29.08		783.10	0.0484	-26.1	0.061	27.9
	580.83	0.07	-25.83	nd		831.00	0.906	-29.31		788.15	0.0827	-25.6	1.5	19.7
	582.74	0.1	-25.42	20.93		831.25	0.312	-28.38		793.70	0.314	-26.6	0.68	24.9
	585.00	0.24	-24.66	15.49		832.83	0.585	-28.92		799.10	1.98	-29.1	2.3	24.9
	585.60	0.21	-24.80	16.5		833.73	0.643	-28.63		799.25	1.53	-25.2	1.1	26.7
	585.80	0.12	-25.40	14.48		833.88	0.234	-25.32		799.39	1.72	-25.2	0.0087	23.3
	586.20	0.22	-23.24	19.99		835.29	0.518	-28.64		799.97	0.0410	-24.1	0.85	8.51
	587.84	1.47	-25.06	26.4		836.36	0.375	-28.95		800.12	0.142	-23.6	2.1	30.6
	589.90	1.45	-25.66	30.07		837.00	0.806	-29.31		800.60	1.31	-25.1	0.078	18.4
	590.50	1.5	-25.42	29.13		838.87	0.845	-28.75		801.34	1.05	-25.3	1.0	30.0
	591.34	3.73	-24.84	nd		838.92	0.234	-28.37		802.67	1.69	-25.6	2.3	27.3
	592.23	1	-25.23	30.1		839.58	0.195	-28.31		803.82	0.890	-25.4	1.7	25.2
	593.20	0.44	-24.48	34.69		841.35	0.208	-28.14		804.43	1.79	-25.1	2.2	25.3
	593.28	0.65	--	35.52		841.55	0.26	-28.85		804.63	0.675	-25.2	--	26.5
	593.47	0.46	-24.37	27.02		844.00	0.494	-29.80		806.02	2.45	-26.6	1.2	16.1
	594.04	1.68	-24.85	28.81		844.79	0.455	-30.04		807.75	0.431	-25.6	0.51	27.7
	595.42	1.12	-25.18	26		845.29	1.19	-30.74		808.32	0.750	-26.0	0.61	24.3
	596.20	0.44	-24.88	26.85		846.53	0.844	-30.37		809.12	0.831	-25.4	0.88	23.9
	596.33	--	-25.32	27.18		847.69	3.42	-29.90		810.15	0.420	-25.9	0.56	26.3
	596.85	--	-25.79	28.7		848.00	2.62	-29.76		810.55	1.90	-26.3	3.2	23.0
	597.43	0.13	--	28.86		848.90	2.16	-29.73		811.75	3.03	-25.8	1.0	20.2
	598.10	0.15	-26.02	19.52		850.12	2.4	-29.75		813.05	1.91	-26.3	0.63	16.8
Morro do Calcário Fm.	606.80	nd	nd	23.48		851.15	2.53	-30.12		814.17	1.82	-25.2	1.1	18.2
	607.78	nd	nd	20.33		850.12	2.4	-29.75		814.53	0.479	-25.8	0.27	22.4
	607.84	nd	nd	21.38		851.15	2.53	-30.12		815.08	0.643	--	0.050	14.4
	608.70	nd	nd	nd						816.95	0.507	-25.9	1.3	20.4
	610.52	nd	nd	8.77						818.00	2.09	-27.0	1.7	10.2
	611.58	nd	nd	-1.97						818.23	1.06	-26.9	2.1	15.8
	612.23	1.57	-25.56	14.72						820.20	0.0802	-25.0	nd	nd
	613.13	1.65	-25.76	23.66						825.25	0.221	-12.5	0.25	11.5
	614.27	0.543	-25.74	19.9						830.00	0.0650	-20.2	1.5	--
	616.20	0.596	-21.82	nd						835.40	0.282	-23.1	0.49	9.70
	619.69	0.021	-21.08	nd										
	620.09	0.9	-28.99	-1.89										
	622.46	1.33	-29.90	3.29										
	624.86	1.38	-30.04	-1.83										
	627.72	0.484	-24.71	3.2										
	628.43	0.578	-26.75	nd										
	638.17	3.43	-23.20	-5.84										
	638.69	0.431	-25.15	-13.03										
	639.38	1.12	-26.11	-2.46										
	640.89	0.364	-25.14	nd										
	642.05	2.82	-27.07	1.1										
	644.05	4.04	-26.43	nd										
	648.61	0.382	-23.34	nd										
	649.32	0.191	-22.57	1.45										
	651.31	0.214	-22.56	nd										
	655.02	0.56	-24.48	-4.82										
	658.16	1.27	-27.51	5.7										
	662.25	3.26	-28.85	5.25										
	667.29	0.672	-28.24	nd										
	668.73	1.6	-29.07	5.25										
	674.09	1.19	-29.03	15.61										
	676.12	2.19	-29.73	9.88										
	677.55	2.06	-29.37	7.32										
	680.82	1.52	--	8.45										
	683.69	2.42	-30.06	nd										
	688.14	1.29	-29.54	8.26										
	691.32	3.82	-29.37	3.15										
	696.27	1.91	--	4.01										

Table 3

	Depth (m)	FeT	Fecarb	Feox	Femag	Fe-AVS	Fepy	FeHR	FeHR/FeT	Fe-S/FeHR
Morro do Calcário Fm.	749.03	1.521	0.655	0.196	0.154	nd	0.236	1.241	0.816	0.190
	752.35	2.369	0.856	0.268	0.179	nd	0.601	1.904	0.804	0.316
	756.20	3.116	1.442	0.463	0.305	0.002	0.155	2.365	0.759	0.066
	759.55	2.235	0.324	0.063	0.062	nd	0.072	0.521	0.233	0.138
	764.47	2.132	0.302	0.104	0.061	0.004	0.075	0.542	0.254	0.146
	769.75	2.243	0.725	0.194	0.116	nd	0.094	1.129	0.503	0.083
	774.20	2.221	0.077	0.075	0.030	nd	0.031	0.213	0.096	0.146
	779.10	2.015	0.077	0.038	0.023	nd	0.005	0.143	0.071	0.035
	783.10	0.944	0.527	0.145	0.093	0.002	0.137	0.902	0.956	0.154
	788.15	3.169	0.608	0.129	0.157	nd	1.499	2.393	0.755	0.626
	793.70	0.502	0.359	0.082	0.025	nd	0.001	0.467	0.930	0.002
	799.10	2.301	1.032	0.220	0.307	nd	0.384	1.943	0.844	0.198
	799.25	3.564	0.012	0.031	0.011	nd	2.077	2.131	0.598	0.975
	799.39	2.442	0.011	0.025	0.008	nd	1.344	1.388	0.568	0.968
	799.97	1.717	0.600	0.178	0.265	nd	0.064	1.107	0.645	0.058
	800.12	1.199	0.322	0.079	0.067	nd	0.526	0.994	0.829	0.529
	800.60	4.938	0.007	0.023	0.007	nd	1.069	1.106	0.224	0.967
	801.34	1.542	0.004	0.020	0.007	nd	0.517	0.548	0.355	0.943
	802.67	2.133	0.008	0.027	0.005	nd	0.899	0.939	0.440	0.957
	803.82	3.392	0.118	0.041	0.043	nd	0.996	1.198	0.353	0.831
	804.43	2.521	0.023	0.027	0.001	nd	0.908	0.959	0.380	0.947
	804.63	3.416	1.128	0.245	0.337	0.004	0.193	1.903	0.557	0.104
	806.02	2.174	0.068	0.036	0.026	nd	0.824	0.954	0.439	0.864
	807.75	3.483	0.381	0.101	0.145	nd	0.561	1.188	0.341	0.472
	808.32	2.961	0.160	0.040	0.048	nd	0.653	0.901	0.304	0.725
	809.12	3.319	0.178	0.080	0.064	nd	0.793	1.115	0.336	0.711
	810.15	1.739	0.184	0.069	0.059	nd	0.443	0.755	0.434	0.587
	810.55	4.605	0.233	0.085	0.074	nd	1.674	2.066	0.449	0.810
	811.75	1.802	0.088	0.054	0.044	nd	0.668	0.854	0.474	0.782
	813.05	3.071	0.208	0.072	0.095	nd	0.168	0.543	0.177	0.309
	814.17	2.329	0.148	0.063	0.033	nd	0.814	1.058	0.454	0.769
	814.53	1.858	0.032	0.041	0.013	nd	0.314	0.400	0.215	0.785
	815.08	3.138	1.102	0.291	0.256	0.006	0.693	2.342	0.746	0.298
	816.95	2.082	0.018	0.022	0.002	nd	0.064	0.106	0.051	0.604
	818.00	2.353	0.563	0.128	0.169	nd	0.439	1.299	0.552	0.338
	818.23	0.836	0.278	0.075	0.079	0.007	0.290	0.722	0.864	0.411
	820.20	6.482	0.247	0.076	0.044	nd	1.878	2.245	0.346	0.837
	825.25	0.700	0.381	0.107	0.057	nd	0.085	0.630	0.900	0.135
	830.00	2.768	0.862	0.188	0.196	nd	1.056	2.302	0.832	0.459
	835.40	0.850	0.407	0.088	0.078	nd	0.208	0.781	0.919	0.266